Università degli Studi di Ferrara

DOCTORAL COURSE IN

"MOLECULAR MEDICINE"

CYCLE XXXIV

COORDINATOR Prof. FRANCESCO DI VIRGILIO

INNOVATIVE DRUG DELIVERY SCAFFOLDS AS NOVEL THERAPEUTIC STRATEGY FOR BONE TISSUE REGENERATION AND TREATMENT OF OSTEOSARCOMA

Scientific/Disciplinary Sector (SDS) BIO/13

Candidate

Dr. Lanzillotti Carmen

_____

(signature)

Supervisor

Prof. Martini Fernanda

_____

(signature)

Years 2018/2021

INDEX

1. INTRODUCTION

1.1. Bone diseases

More than 20 million people in the world are annually affected by bone disease inducing loss of bone tissue [1].

Trauma and bone healing complications relate to several factors including age, gender, and infectious agents, as reported in diagnoses. These, include osteoporosis, osteopenia and severe dental problems causing loss of teeth [2].

Osteoporosis represents a global public health concern as it affects approximately 50 million people in industrialized countries [3]. It is characterized by an imbalance in the bone remodelling process leading to a progressive loss of bone mass, which in turn represents an increased fracture risk. Osteoporotic patients suffer from a reduction in their quality of life due to decreased functional mobility, which has indirect consequences on society as a whole [4]. Bone fractures and injuries are also caused by sarcopenia, a common geriatric syndrome, which causes a progressive reduction in muscle mass. This condition is often associated with osteoporosis when it is known as sarco-osteopenia or sarco-osteoporosis, leading an increased risk of bone fracture [5].

Bone cancer is a chronic bone disease that represents the second most common cause of cancer mortality in the world. Osteosarcoma (OS) is the most recurrent type of bone cancer of such malignancies, including chondrosarcoma and Ewing's sarcoma, as described below.

1.2. Osteosarcoma

OS is the most common of malignant bone cancers, which is mainly diagnosed in children and adolescents [6]. It consists in the production of osteoid and bone from malignant spindle cells [7]. The most common subtype is conventional high grade OS, which mainly affects pediatric patients and young adults. OS has a bimodal age distribution, with the first peak in children and young adults occurring between 10 - 30 of age and a second peak in the elderly from 70 - 80 years of age [8]. The first peak corresponds with the pubertal growth spurt suggesting a relationship between this occurrence and bone proliferation [9]. The second peak in OS is represented by secondary bone lesions, often related to Paget's disease, different radiation therapies or a genetic predisposition to syndromes including retinoblastoma 1 [6,10]. However, emerging evidence has revealed that the 50% of OS in elderly individuals appears *de novo* without pre-existing bone diseases [10]. OS rarely occurs in children younger than 5 years old and, in this case, is associated with a cancer susceptibility syndrome known as Li-Fraumeni syndrome [6].

The overall annual incidence of this OS type is 4.7 per cases [11], although it increases in adolescents where the annual incidence rate is 8-11 million per year [11]. Moreover, OS is 1.4 times more frequent in males than in females [9] and in Afro-Americans and Hispanics than Caucasians [11]. The 5-year survival rate for OS is 70%, as reported by the American Cancer Society. It represents the cause of 8.9% of cancer-related deaths; the survival rate correlates the patients' ages [11].

Although OS can begin in any bone, the metaphyseal growth plates of the long bones are the most affected sites, with 42% of cases in distal femur, 19% in proximal tibia, and 10% in proximal homerous [12]. Other affected areas are the jaw (8%), the pelvis (8%) [11] and the ribs (1,25%) [12]. 5% of all primary OS develops in the spine, mainly affecting individuals of 10-20 years old [13].

OS develops in a radial manner, forming a ball-like mass that penetrates the bony cortex and compresses the surrounding muscles. Nodules or satellites may arise from this primary structure, with a pseudo-capsular layer, known as the reactive zone, inducing pain and, in some cases, pathological induced fractures in patients [7]. Since OS manifestation is highly heterogeneous [14], the World Health Organization has histologically classified OS into central, intramedullary and surface tumours with subtypes for each group, including conventional OS, telangiectatic OS, small-cell OS, low-grade OS, parosteal OS, periosteal OS, and high-grade surface OS [15].

Surgery is the primary treatment for OS consisting in the removal of the tumour mass. Surgical resection involves the affected tissue including areas where biopsies or drainage have occurred, as well as other potentially contaminated tissues. Often entire limbs are removed [16].

Spine surgery is a risky undertaking due to the unique anatomy of the anatomical district and its relationship with the surrounding neural and vascular structures. Surgery on growing children with immature skeletons can create significant limb-length discrepancy and gait abnormalities [17]. Chemotherapy is combined with surgery for OS treatment in order to ensure the eradication of malignancy and is given before and after surgery [6]. Neoadjuvant chemotherapy associated with intercalated surgery represents the standard of care for OS [18]. In addition, although the choice of chemotherapy drugs is still controversial, methotrexate, doxorubicin (Adriamycin) and cisplatin are the preferred option to treat conventional OS [18]. Specifically, the most commonly employed chemotherapeutic agents are high-dose methotrexate and doxorubicin [16,19]. Accordingly, the American standard protocol for treating OS provides for induction chemotherapy with high-dose methotrexate and/or doxorubicin for 10 weeks before and 17 weeks after the surgery [6]. This therapeutic scheme is also employed in the Istituto Ortopedico Rizzoli, Bologna, Italy [20]. During primary treatment, patients receive high-

dose methotrexate (12 g/m^2), doxorubicin (75 mg/m^2) and cisplatin (120 mg/m^2), while receiving two cycles of doxorubicin (90 mg/m^2) and three cycles each of high-dose methotrexate, and cisplatin (120 to 150 mg/m^2) in the post-operative phase [19]. To this end, it is important to note that the high-dose methotrexate standardly used in clinics (8–12 g/m^2) is much higher than the lethal dose (2–4 mg/kg). Although leucovorin is widely co-administered to reduce the toxic effects of administered methotrexate, therapy is still harmful to patients [19]. Moreover, although prognosis for patients with localized OS (event-free-survival up to 70%), has improved with multimodal therapy that combines surgery with pre- and post-operative chemotherapy, outcome for patients with metastatic OS is still poor [21].

OS treatment may present complications due to the toxicity of chemotherapeutic agents and after effects. The most frequent of these are alopecia, myelosuppression, mucositis, nausea, and vomiting, whereas the after effects include cardiac toxicity, acute and chronic nephrotoxicity, neurotoxicity, hearing loss, infertility, and second malignant neoplasms [22]. In addition, chemotherapy uses drugs to rapidly kill dividing cancer cells, as well as healthy dividing cells [21].

Although prognosis has improved a little for patients, there are still different opinions on optimal treatment options. Therefore, new treatment combinations or methods are needed. This need has motivated research into new therapy strategies including scaffolds with drug-delivery system.

1.3. Scaffolds for bone tissue repair

Bone tissue in physiological conditions has the ability to regenerate itself. However, bone fractures due to injuries, trauma and/or bone diseases can compromise healing capacity. For this reason, there is a clinical need to substitutes the damaged or lacking tissue. Nowadays, autograft and allograft represent the therapeutic strategy to restore bone loss

despite several disadvantages. Autograft is limited by the bone volume that can be harvested from the iliac crest and by surgical risks, such as bleeding, inflammation, infection, chronic pain, and damage to the donor site, whereas allograft is limited by lack of donors, high costs, the need for sterilization and the risk of infectious agent transmission or immune mediated tissue rejection [23].

In this scenario, with a need for clinical alternative therapeutic strategies, new biomaterials/scaffolds in combination with stem cells and growth factors have been employed for bone repair leading to improved patient outcomes. Furthermore, the bone substitutes may represent an effective clinical strategy to solve discrepancy in bone tissue which is caused by tumour surgical resection, fractures and trauma, thus preventing healing failures.

Several studies in tissue engineering combined with regenerative medicine have attempted to develop scaffolds, which are similar to bone structure and composition with cytocompatibility and osteoinductivity properties in order to induce cell proliferation and osteogenic differentiation in the affected sites. To this purpose, should be remembered that bone is composed of: (i) 50–74 wt% mineral phase (mainly HA 45–58%, carbonate ~4%, citrate ~0.9%, sodium ~0.7%, magnesium ~0.5%, and many other trace elements, such as F^-, K^+, Sr^{2+}, Pb^{2+}, Zn^{2+}, Cu^{2+}, Fe^{2+}), (ii) 16–40 wt% organic phase (85–90% collagen) and (iii) 10 wt% water [4].

Bone and joint substitutes are commonly made of metals, ceramics, polymers, and their composites [24]. In most of the cases, ceramics, polymer and composite biomaterials are used in bone regeneration applications. Ceramics present biocompatibility with the human organism, as well as is resistance to compression and corrosion; nevertheless, this material is also brittle and has low strength [25]. Ceramic scaffolds are commonly composed of calcium phosphate (CaP) and tricalcium phosphate (TCP) enriched with cationic substitution such as Sr^{2+} or Mg^{2+}, to improve mechanical and chemical/physical

properties. Due to their excellent bioactivity, an increasing interest on the development of calcium phosphate bone cements (CPCs) is being expressed in literature. In particular, the synthesis of CPCs based on the hydrolysis and transformation of α-Ca3(PO4)2 (αTCP) into nanostructured calcium-deficient hydroxyapatite (CD-HA) particles is being estimated. In addition, CD-HA doped with Sr^{2+} ions seem to be effective against osteoporotic bone damage [26].

Polymer scaffolds can be natural or synthetic. Collagen and chitosan are natural polymers, which mimic natural bone structure, despite inadequate thermal stability. In addition, since collagen does not exhibit good mechanical properties, it is combined with ceramic scaffolds [27–29]. On the other hand, synthetic polymers include poly ("-caprolactone) (PCL), polylactic acid (PLA), polyglycolide (PGA) and the copolymer of poly-(DL-lactic-co-glycolic-acid) (PLGA). However, these polymers appear unsuitable for bone tissue regrowth and show disadvantages due to their degradation [30,31].

Composite scaffolds are a combination of polymers and ceramics biomaterials. Recently, some studies have aimed at evaluating the biocompatibility and osteoinductivity of composite scaffolds, which employ mesenchymal stem cells. Among these, the scaffold composed of hydroxyapatite (Pro Osteon 200) and collagen (Avitene) known as Coll/Pro Osteon200, the scaffold made of Polylactide β-tricalcium phosphate (PLLA/β-TCP) matrix grafted with gelatine/hydroxyapatite, and the biomaterial consisting of poly (ε-caprolactone)/tricalcium phosphate (PCL/TCP) with carbonated hydroxyapatite (CHA)-gelatin composite showed good biocompatibility and osteoinductivity features proving themselves suitable for bone tissue repair [32–34].

1.4. Drug-delivery scaffolds for osteosarcoma treatment

Bone dysfunction due to bone diseases has become a major problem for our society affecting more than 20 million people per year [1,35]. Regeneration bone fractures, resulting from trauma, osteoporosis or tumours, is a major problem in our super-aging society. Moreover, bone cancer, in particular OS, can affect any skeletal bone leading to death in children and young adults. Surgery in combination with chemotherapy is the first line treatment for OS, as described before. After tumour mass resection, major problems are (i) regeneration of bone structure to address aesthetic and functional activities, and (ii) preventing cancer relapse [36]. In recent decades, the former has tended to be solved with hydroxyapatite (HA), which is used for bone regrowth due to its slow resorption ability and composition, similar to natural bone [36]. Indeed, the use of bone substitutes allows to fill the surgery-caused gap in damaged bone tissue that cannot be able to heal physiologically. The problem of cancer recurrence is a more complicated challenge. Pre- and post-operative chemotherapy often results in adverse effects reducing the patients' quality of life [36]. Furthermore, only the 5% of the injected drugs is targeted on tumour site [37,38].

A drug-delivery system is necessary to prevent offside effects and improves treatment efficacy. Indeed, locally delivering anti-cancer compounds improves on high local concentrations with more efficient tumour killing effects, reduced drugs resistance and confined systemic effects. In addition, as antineoplastic agents are not degraded by the metabolism during circulation, therapeutic effectiveness is increased with lower doses [39].

Therefore, implantable drug-delivery scaffolds, which combine anti-cancer molecules and bone substitutes, constitute a major area of investigation for this scientific field [40].

Polymers, ceramics and their composite materials are used to create such drug delivery systems. Since 1991, proposals have included PLGA, chitosan, polyurethane, alginate, poly-L-lactic acid, PEG–poly polymers in combination with doxorubicin, cisplatin, curcumin, paclitaxel, and ellagic acid, as reviewed [41].

Nevertheless, HA is most extensively used in the CaP phase due to such materials representing eligible physical/chemical properties for such a drug-delivery approach. Indeed, HA has been used in combination with collagen and different platinum complexes [42–44]. For example, collagen (COLL)/HA/cisplatin-derived scaffolds, which are just such composite biomaterials, are used in drug-delivery systems [45,46].

In addition, a new paclitaxel-loaded HA/alginate composite material has been developed for the treatment of metastatic spine cancer with promising *in vivo* results in terms of survival time [41].

Recently, super-para-magnetic iron-doped nanocrystalline apatite (FeHA) has been developed as a delivery system for doxorubicin and methotrexate with promising *in vitro* results for treating OS [40,47].

At present, no information is available in literature about the use of strontium-substituted CD-HA, as a carrier of anticancer agents including methotrexate and doxorubicin.

1.5. *In vitro* study models

1.5.1. Mesenchymal Stem Cells

Bone regeneration processes may be improved with the use of mesenchymal stem cells (MSCs). Therefore, MSCs together with biomaterials/scaffolds and growth factors are often employed in regenerative medicine to accelerate bone healing at the fracture site. Indeed, MSCs are promising competent biomedical candidates in the regenerative medicine field [48,49].

Indeed, MSCs have several important biological properties, such as the capacity to secrete molecules that can induce tissue regeneration, self-renewal and proliferation, as well as multipotentiality, anti-inflammatory and immunomodulatory effects [48,50–52]. Isolated initially from bone marrow (BM) [53], MSCs have subsequently been harvested from different anatomical regions, such as adipose tissue (ASCs) [54,55], the umbilical cord (UC-MSCs) [56], dental pulp tissues (DPSCs) [57], and others [57–60]. MSCs play a key role in the natural events leading to bone repair and healing by differentiating into osteoblasts, which secrete a regenerating bone matrix. Due to their biological ability to differentiate into osteoblasts, MSCs are also attractive candidates for bone tissue engineering approaches and in the management of several bone disorders [61].

Regenerative events naturally occur in damaged tissue to allow local repair and bone healing to take place [62]. The first is the local and systemic release of pro-inflammatory cytokines and the recruitment of immune cells inducing soft-tissue inflammation and edema. Subsequently, callus formation and bone remodelling take place starting from the differentiation of osteogenic progenitor cells and the local release of bone morphogenetic proteins. The migration of endogenous or exogenous MSCs to the bone injury site is a crucial step in treating bone disease [48]. Specifically, endogenous MSCs are recruited to the site in question by inflammatory mediators secreted by immune cells including Transforming Growth Factor β1 (TGF-β1) and stromal cell-derived factor 1 (SDF-1 also known as CXCL12) [63,64]. The most common clinically employed MSCs are human adipose-derived mesenchymal stem cells (hASCs) and bone-marrow-derived mesenchymal stem cells (BM-MSCs) [65]. Nevertheless, BM-MSCs collection from patients is painful and results in bleeding and infections. Moreover, BM-MSCs show altered proliferation and senescence with increasing age. On the other hand, hASCs do not present negative age-related effects, whereas their collection is much less painful than for BM-MSCs [48]. HASCs may be obtained in more abundant numbers than BM-MSCs

[48]. In recent decades, scientific studies have been conducted using hASCs for bone tissue engineering regeneration/regrowth and to evaluate the *in vitro* biocompatibility and osteoinductivity properties of scaffolds [33,55,66,67].

1.5.2. Osteosarcoma cell lines

Cancer cell lines are required to better characterize the mechanisms behind carcinogenesis, functional characteristics of genes and drug discovery, screening and response [68]. Osteosarcoma cells are derived from malignant bone tumours and, despite their osteoblastic features, they present chromosomal alterations which cause abnormal molecular and cellular functions [69]. In scientific research field, about twenty cell lines are used to well define the homonymous disease. Human osteosarcoma cell lines can be divided into fibroblastic and osteoblastic subtypes. The osteosarcoma fibroblastic subtype is shared by U-2 OS, OSA, MG-63, IOR-OS10, MHM, whereas the osteoblastic one is common to SAOS-2, IOR-OS14/15/18, KPD, OHS, ZK-58 and G292. The osteosarcoma subtype of HOS, HOS-143B/MNNG, IOR-MOS/OS9, SARG and HAL cell lines is unknown [68–70]. Furthermore, the MG-63, U-2 OS and SAOS-2 cell lines were also characterized through cellular biology assay confirming the heterogeneous and immature osteoblastic features of MG-63 and U-2 OS cells, respectively and revealing the SAOS-2 the cells with the most mature osteoblastic profile [69].

Due to their features, SAOS-2, represents the most suitable *in vitro* cellular model for investigating mechanisms behind OS. SAOS-2 was derived from the malignant bone tumour of a Caucasian female of 11 years old [71]. The characterization of these cells revealed that osteoblastic-like features are shared [69,72]. For this reason, SAOS-2 cell line has been employed in several scientific studies, as a cellular model for assessing biological parameters [73–76]. In addition, SAOS-2 cells were previously genetically engineered in our laboratory to constitutively express the enhanced green fluorescent

protein (eGFP), as a reporter gene [75]. This engineered cell line was named SAOS-eGFP cells and is used in many study models since some analyses are simplified by fluorescent detection [51,73,74,76,77].

2. AIMS

Many studies have been carried out in the effort to identify substitutes for the bone regrowth. However, little is known about the biological, genetic and epigenetic effects of adding substitutes to bone. The biological parameters of cells grown on bone-substitutes should be known before proposed scaffolds are clinically employed.

Moreover, an increasing number of people are annually affected by bone diseases. Indeed, OS is the second cause of death worldwide. Nowadays, OS treatment is still controversial and often inefficient in the entire globe. Therefore, there is a clinical need for therapeutic strategies in bone regeneration and OS treatment.

Overall, the main objective of the present study was to characterize an innovative ceramic scaffold composed of strontium-substituted nanostructured calcium-deficient hydroxyapatite (CD-HA 2%Sr) in order to evaluate its cytocompatibility and osteoinductivity. In addition, CD-HA 2%Sr scaffolds linked with anti-cancer drugs such as methotrexate and doxorubicin were tested for their ability to contrast the proliferation of OS cells.

Aim I: To evaluate the cytocompatibility of CD-HA 2%Sr scaffold, hASCs were grown on the scaffold, up to day 14. To this purpose the biomaterial was subjected to Scanning Electron Microscopy analysis, while hASCs were investigated for viability, morphology, cytoskeleton architecture and gene expression profile.

Aim II: To evaluate the osteoinductivity of CD-HA 2%Sr scaffold in hASCs grown on the scaffold, up to day 14, osteogenic markers were investigated in terms of gene and protein expressions, with PCR Array, ELISA test and matrix mineralization analyses.

Aim III: To assess the cytotoxic effect of CD-HA 2%Sr scaffolds, linked to the anti-cancer drugs Methotrexate (CD-HA 2%Sr-MTX) and Doxorubicin (CD-HA 2%Sr-DOX) scaffolds on OS cells proliferation. Engineered human osteosarcoma cell line SAOS-eGFP cells was seeded on the scaffolds, up to day 7. The functionalized scaffolds were subjected to Scanning Electron Microscopy analysis, while the cytotoxic effects of drugs were evaluated investigating cell viability exploiting also the fluorescence emitted by SAOS-eGFP cells.

3. MATERIALS AND METHODS

3.1. Experimental design

The cytocompatibility and osteoinductivity properties of the innovative scaffolds made up of strontium-substituted nanostructured calcium-deficient hydroxyapatite were assessed in hASCs grown on the scaffold, up to day 14. Metabolic activity, cell viability, and cytoskeleton morphology, alongside extracellular matrix gene expression analyses allowed CD-HA 2%Sr scaffold cytocompatibility to be evaluated. On the other hand, the study of mineral matrix deposition along with osteocalcin protein expression and osteogenic genes expression studies allowed to assess the osteoinductivity of the CD-HA 2%Sr scaffold.

The ability of CD-HA 2%Sr scaffolds linked to the anti-cancer drugs Methotrexate (CD-HA 2%Sr-MTX) and Doxorubicin (CD-HA 2%Sr-DOX) to contrast OS cells proliferation was analysed *in vitro* in SAOS-eGFP cells, up to day 7. The effects of released drugs were assessed by evaluating cell numbers and fluorescence intensity rate reductions in the engineered SAOS-eGFP cells grown on the biomaterials.

The structure of CD-HA 2%Sr, CD-HA 2%Sr-MTX, and CD-HA 2%Sr-DOX scaffolds, with cells grown on them, was analysed by scanning electron microscope.

3.2. Cell cultures

Cryopreserved frozen hASCs, at the first passage, were purchased from Lonza (Lonza, Milan, Italy). These hASCs are positive for CD13, CD29, CD44, CD73, CD90, CD105, CD166 surface markers, whereas other markers including CD14, CD31, and CD45 are absents, as expected. Cells were cultured at a density of 5,000 cells/cm^2, in a T75 flask

(Falcon BD, Franklin Lakes, NJ, United States) in minimum essential medium – Alpha-MEM Eagle with Earle's BSS (α-MEM; Lonza, Milan, Italy) supplemented with 10% foetal bovine serum (FBS; Bio Whittaker, Milan, Italy), 2% penicillin/streptomycin (Pen/Strep 10,000 U/ml; Sigma, Milan, Italy). Cells were maintained in a humidified atmosphere at 37°C with 5% CO_2. HASCs were seeded with a concentration of 1.5 x 10^4 cells per well and were grown on (i) CD-HA 2%Sr scaffolds and (ii) tissue culture polystyrene (TCPS) vessels until analyses day.

The SAOS-eGFP engineered cells were derived from parental SAOS-2 cells [75]. Cells were expanded in Dulbecco's Modified Eagle Medium F-12 (DMEM/F12; Lonza, Milan, Italy) with 10% FBS and 1% of Geneticin (Invitrogen, Milan, Italy) and kept in a humidified atmosphere at 37°C with 5 % CO_2 as reported [74]. SAOS-eGFP cells were seeded with a concentration of 1.5 x 10^4 cells per well and were grown on (i) CD-HA 2%Sr, (ii) CD-HA 2%Sr-MTX, and (iii) CD-HA 2%Sr-DOX until analysis day.

3.3. Biomaterial Composition

The biomaterials tested herein are designed as bioactive injectable bone cements with drug delivery abilities, which may contrast OS and spine tumour recurrences, while favouring healthy bone regrowth. The scaffolds derive from calcium-phosphate bone cements (CPCs) precursors and consist of strontium substituted nanostructured calcium-deficient hydroxyapatite (CD-HA 2%Sr) enriched with sodium alginate.

The scaffolds synthesis and functionalization were made at the Institute of Science and Technology for Ceramics, National Research Council (ISTEC-CNR), Faenza, Italy by the Bioceramics and Bio- hybrid Composites Group, as previously reported [26,40,47]. The CD-HA 2%Sr scaffolds were functionalized with anti-cancer drugs Methotrexate (CD-HA 2%Sr-MTX) and Doxorubicin (CD-HA 2%Sr-DOX).

Specifically, CD-HA 2%Sr-MTX and CD-HA 2%Sr-DOX scaffolds were prepared in order to release different drug concentrations daily, up to day 7, as shown in Tables 1 and 2, respectively.

Table 1. Methotrexate concentration detected up to 7 days and Standard Deviation

Day	µg/mL	Standard Deviation
1	45.67	10.91
2	47.25	12.34
3	47.39	12.31
4	47.55	12.46
7	47.87	12.63

Table 2. Doxorubicin concentration detected up to 7 days and Standard Deviation

Day	µg/mL	Standard Deviation
1	1.70	0.27
2	2.94	0.50
3	4.17	0.55
4	5.18	0.42
7	7.11	0.67

Drug adsorption experiments on CD-HA 2%Sr substrate were carried out using a solid-solution ratio equivalent to 20 mg of apatite in 5 ml of drug solution at increasing concentrations (0,45 - 50 μg/ml for MTX and 0,54 – 54 μg/ml for DOX). The amount of drug adsorbed (Q_{ads}) for any data-point was determined by comparing the amount of drug remaining in solution after the adsorption experiment to the initial concentration. Drug being directly titrated by visible spectrophotometry with absorption at λ = 372 (MTX) and 496 nm (DOX) using a Cary Bio spectrophotometer (Varian, Palo Alto, USA). KCl 0.01 M was used as a solvent in all experiments to provide a nearly constant ionic strength with a calibration curve as reference of drug concentration. Adsorption experiments were carried out at 37 °C ensuring an optimal interaction between the surface of the apatite substrates and the solution. Afterwards, the system was centrifuged at 5000 rpm for 5 min for retrieval of the solid and for drug quantification followed by Raman micro-spectrometry to analyse the adsorption. In order to study the drug-kinetics release of MTX and DOX, drug-CD-HA 2%Sr samples were immersed in 2 mL of HEPES 0.01 M at pH 7.4 in KCl 0.01 M, and daily analysed with a spectrophotometer at 306 nm and 480 nm, respectively. The latter investigation was carried out at ISTEC-CNR (Faenza, Ravenna, Italy) providing us data showed in Figure 1.

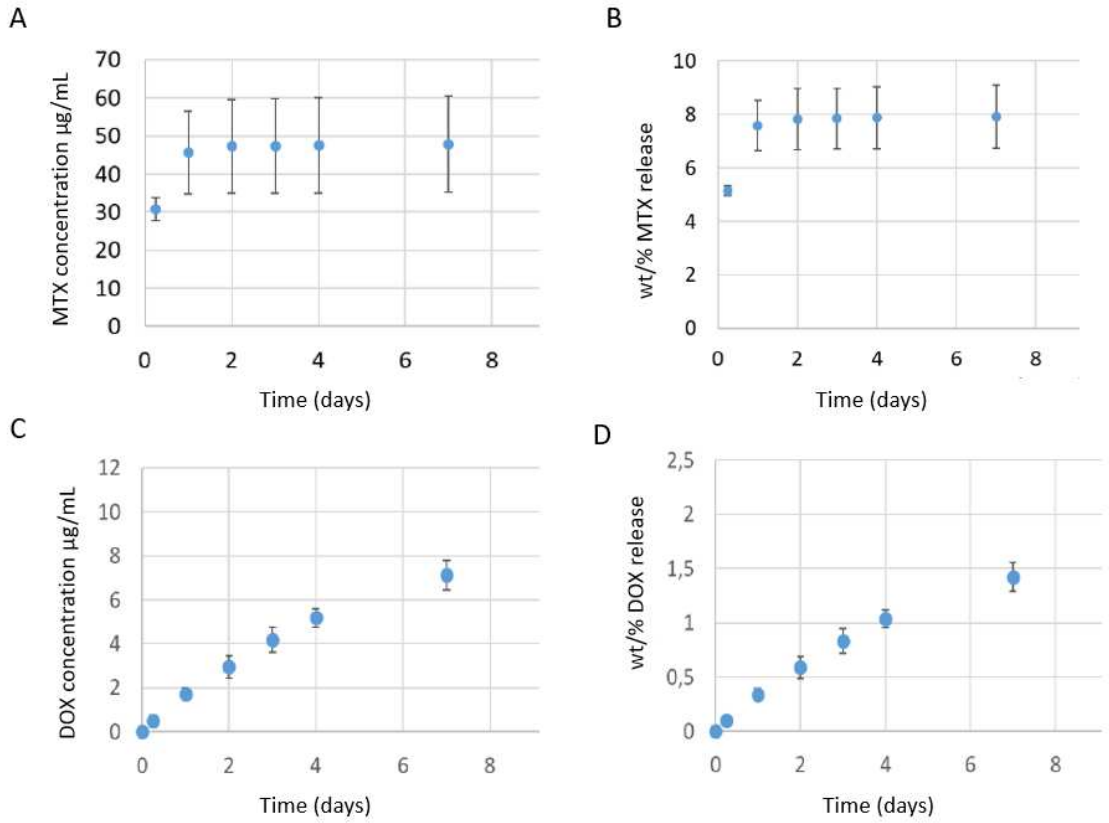

Figure 1. MTX/DOX-release kinetic study. A) and C) µg/mL of MTX and DOX released from CD-HA 2%Sr scaffold up to day 7. B) and D) wt% of MTX and DOX released from CD-HA 2%Sr scaffold up to day 7.

Biological assays were carried out at the University of Ferrara, Department of Medical Sciences. Before beginning the cell seeding, scaffolds were sterilized with two washes of ethanol 70% (20 min/each) and ultraviolet (UV) light (30 min/side) and kept in 5 mL of medium at 37°C for 3 days. The disk-shaped samples had a diameter of 10 mm and a height of 2 mm.

3.4. Scanning Electron Microscopy Analysis

Scanning electron microscope (SEM) analysis was carried out to investigate the structure of CD-HA 2%Sr, CD-HA 2%Sr-MTX, and CD-HA 2%Sr-DOX biomaterials and to analyse cell-cement interaction. To this purpose, hASCs (1.5×10^4) were grown on CD-HA 2%Sr scaffold up to day 14, while SAOS-eGFP cells (1.5×10^4) were grown on CD-

HA 2%Sr, CD-HA 2%Sr-MTX, and CD-HA 2%Sr-DOX scaffolds up to day 7. After cells culture, scaffolds were washed with PBS and fixed for 1 h by 2.5% glutaraldehyde and 4 h by 1% osmium solution in phosphate buffer. Samples were sputter-coated with gold and observed with SEM (Cambridge United Kingdom, model Stereoscan S-360) [49].

3.5. Cytocompatibility analysis of CD-HA 2%Sr scaffold

The hASCs (1.5 x 10^4 cells) were seeded onto CD-HA 2%Sr scaffold and on TCPS in order to analyse the effect of the biomaterial on cell viability. Alamar Blue, Live/Dead assays, analysis of cytoskeleton architecture, and extracellular matrix genes expression analyses were performed for hASCs grown on (i) CD-HA 2%Sr and (ii) TCPS, as control, at different time points based on the analysis type.

Alamar Blue assay. The metabolic activity rate of hASCs grown on the scaffolds and controls was determined using the Alamar Blue assay (Invitrogen, Milan, Italy) at day 1, 2 and 7. The cells were incubated in medium with 5% of Alamar Blue reagent for 3 hours at 37°C. A concentration of 1.6 x 10^5 cells and serial 1:2 dilutions were seeded to generate a calibration curve consisting in scalar concentrations of hASCs at up to 5,000 cells. Subsequently, supernatant optical density was measured at a 570 nm wavelength and at a 620 nm reference wavelength using a spectrophotometer (Thermo Electron Corporation, model Multiskan EX, Helsinki, Finland) [49]. The analysis was performed in triplicate for each experimental group.

Live/Dead Assay. The cytocompatibility of hASCs grown on CD-HA 2%Sr scaffold was assessed by live/dead dye and confocal laser scanning microscopy analyses, at days 3, 6 and 14. Live/Dead Cell Double Staining Kit (Calbiochem, Milan, Italy) was used to analyse the viability of hASCs grown on the biomaterial. Live/Dead assay was performed

according to the manufacturer's instructions. Cell-permeable green fluorescent Cyto-dye (Ex. max.: 488 nm; Em. max.: 518 nm) was used to stain live cells, whereas propidium iodide (Ex. max.: 488 nm; Em. max.: 615 nm) was used to stain dead cells. Scaffolds were kept in saline solution during the confocal microscope analysis (LSM510; Carl Zeiss, Jena, Germany) using a 10 × 1.4 NA Plan- Apochromat oil-immersion objective and equipped with ZEN microscope imaging software (Zeiss Instruments). Digital images were acquired in z-stacks at 0.5 μm. Moreover, the Live/Dead assay was performed in cells grown on glass slides in contact with CD-HA 2%Sr scaffolds and on TCPS, as control. Digital images were acquired by the TE 200-E fluorescent microscope using ACT-1 software for DXM120F digital cameras (Nikon Instruments, Sesto Fiorentino, Italy) at 20X magnification, then analysed using Image J software [78].

Cytoskeleton architecture. Tetramethyl – rhodamine – iso – thio - cyanate (TRITC) conjugated-Phalloidin (Sigma, Milan, Italy) was used to stain cytoskeleton filaments of hASCs at day 14. The cells grown on glass slides were washed with PBS 1X and fixed with 10% formalin for 10 minutes at room temperature. Afterwards, cell nuclei were marked with 0.5 mg/ml DAPI (Invitrogen, Milan, Italy). The glass slides containing labelled cells were analysed using a TE 200-E fluorescent microscope at 10X and 20X magnification. Images were obtained using ACT-1 software for DXM120F digital cameras (Nikon Instruments, Sesto Fiorentino, Italy). Cell cytoskeleton analysis at 40X magnification was carried out with Olympus Xcellence multiple wavelength high-resolution fluorescence microscopy system (Olympus) and analysed using Image J software [49,79].

3.6. RNA isolation and reverse transcription

HASCs were grown on tested CD-HA 2%Sr scaffold and TCPS control up to day 14. At day 3, 6, and 14, RNA was isolated using the RNeasy Plus Micro Kit (Qiagen, Milan,

Italy) following provided protocol. RNA quality and quantity was evaluated using a nanodrop spectrophotometer (ND-1000, NanoDrop Technologies, Wilmington, DE, USA), then reverse transcribed to cDNA using the RT² First Strand cDNA Kit as recommended (Qiagen, Milan, Italy).

3.7. Human Extracellular Matrix and Adhesion Molecules RT² Profiler PCR Array

A Human Extracellular Matrix and Adhesion Molecules PCR Array (Qiagen, Milan, Italy, Catalog n. PAHS-013Z) was employed to analyse the genes modulated in hASCs from CD-HA 2%Sr scaffolds at days 3, 6 and 14. RT^2 Profiler PCR Array for Extracellular Matrix and Adhesion Molecules allowed to analyse the expression of 84 genes involved in cell-to-cell adhesion, cell to extracellular matrix (ECM) adhesion, and 5 housekeeping genes. Analysis was carried out using the SYBR Green method on a CFX96 Touch™ PCR detection system (Bio-Rad, Milan, Italy). In data analysis, the fold-change of each gene expression was calculated using the $2^{-\Delta\Delta CT}$ method. The housekeeping genes, employed as controls, were used to normalize the results. All reactions were performed in triplicate; twice fold up- or down-regulated expression (Log_2 fold change > 1 or < 1) compared to controls was considered significant [55].

3.8. Osteoinductivity analysis of CD-HA 2%Sr scaffolds

The osteoinductivity propriety of CD-HA 2%Sr scaffold was assessed in hASCs grown on (i) the biomaterial and (ii) TCPS, up to day 14. Alizarin Red Staining and Osteocalcin protein expression analyses, alongside a human osteogenesis RT-PCR Array, were carried out in the two experimental groups at different time points based on the analysis type [49,55].

3.8.1. Alizarin Red Staining assay in hASCs grown on CD-HA 2%Sr scaffold

HASCs grown on CD-HA 2%Sr scaffolds and TCPS for 14 days were fixed in 4% neutral buffered formalin and stained with a 40 mM, pH 4.2 solution of Alizarin Red (Sigma-Aldrich) to analyse mineral matrix deposition. After extensive washing to remove unbound staining pictures were created using a standard light microscope (Nikon Eclipse TE 2000-E microscope, Nikon Instruments Spa, Sesto Fiorentino, Italy) equipped with a digital camera (DXM 1200F; Nikon Instruments Spa, Sesto Fiorentino, Italy). Afterwards, the mineralized substrates were dissolved using 20% methanol and 10% acetic acid in a water solution (Sigma-Aldrich, Milan, Italy), whereas the quantification was carried out in triplicate in cuvettes using spectrophotometer (Thermo Electron Corp., model Multiskan EX, Vantaa, Finland) at a wavelength (λ) of 450 nm.

3.8.2. Osteocalcin protein expression

An ELISA was carried out at day 14 in order to identify osteocalcin (OCN) protein expression in hASCs grown on CD-HA 2%Sr scaffold and TCPS. Protein extraction was performed using Cell Extraction Buffer (Thermo Fisher Scientific, Milan Italy) with 1 mM of phenylmethylsulfonyl fluoride (PMSF), and a protease inhibitor cocktail. Protein concentration was evaluated using bicinchoninic acid (BCA) (Thermo Fisher Scientific, Milan Italy) according to the provided instructions. OCN protein expression was analysed using Human Osteocalcin Instant ELISA (Thermo Fisher Scientific, Milan, Italy) following the provided protocol.

3.8.3. Human Osteogenesis RT^2 Profiler PCR Array

The human Osteogenesis PCR Array (Qiagen, Milan, Italy, Catalog n. PAHS-026Z) was assessed in order to identify genes, which are involved in osteogenic pathways modulated by CD-HA 2%Sr scaffolds in hASCs at day 3, 6 and 14. RT^2 Profiler PCR Array for

human osteogenesis was employed in real-time-PCR to analyse the expression of 84 genes involved in skeletal development and bone mineral metabolism, as well as cell adhesion molecules. In terms of data analysis, the fold change for each gene expression was calculated using the $2^{-\Delta\Delta CT}$ method and then normalized by comparing these values with those of the housekeeping genes, which were used as controls. All reactions were performed in triplicate; twice fold up- or down-regulated expression (Log_2 fold change > 1 or < 1) compared to controls was considered significant.

3.9. Anti-proliferative activity analysis of drug-linked CD-HA 2%Sr scaffolds on SAOS-eGFP cells

The ability of CD-HA 2%Sr-MTX and CD-HA 2%Sr-DOX scaffolds to contrast OS cells proliferation was assessed in SAOS-eGFP cells grown on them up to day 7. SEM (as reported in paragraph 3.3), Alamar Blue, and SAOS-eGFP cells fluorescence intensity analyses were carried out to evaluate anti-proliferative activity in the functionalized scaffolds.

3.9.1. The effects of drug-linked CD-HA 2%Sr scaffolds on SAOS-eGFP cells

The effects of CD-HA 2%Sr-MTX and CD-HA 2%Sr-DOX scaffolds on cells viability were studied in SAOS-eGFP cells by evaluating their fluorescence intensity using confocal laser scanning microscopy and the cell metabolic activity rate with Alamar Blue assays.

SAOS-eGFP cells fluorescence analysis. Digital images of SAOS-eGFP cells grown on CD-HA 2%Sr, CD-HA 2%Sr-MTX, and CD-HA 2%Sr-DOX scaffolds were obtaining using a confocal microscope (LSM510; Carl Zeiss, Jena, Germany) with a 10 × 1.4 NA Plan- Apochromat oil-immersion objective and equipped with ZEN microscope imaging software (Zeiss Instruments). The SAOS-eGFP cells fluorescence intensity mean for each

sample was evaluated using Image J software as previous reported [80–82]. Analysis was performed at day 7.

Alamar Blue assay. The metabolic activity of SAOS-eGFP cells grown on CD-HA 2%Sr-MTX and CD-HA 2%Sr-DOX scaffolds was evaluated using the Alamar Blue assay (Invitrogen, Milan, Italy), employing the same experimental conditions used for hASCs grown on CD-HA 2%Sr biomaterial. Alamar Blue assay was performed with SAOS-eGFP cells (1.5 x 10^4 cells) grown on (i) CD-HA 2%Sr-MTX, (ii) CD-HA 2%Sr-DOX, and (iii) CD-HA 2%Sr, as control. Each experimental group was tested in different time points at day 1, 2, and 7 [83–85].

3.10. Statistical analysis

Statistical experimental analyses, which were performed in triplicate, were carried out using the GraphPad Prism 7.04 software for Windows. Data obtained from the Alamar Blue assay were analysed with 2-way ANOVA and multiple comparison tests. T-test was used to analyse osteocalcin protein expression and matrix mineralization, whereas, statistical analysis of the fluorescence intensity mean was carried out using One-way ANOVA. P-value < 0.05 was considered significant.

4. RESULTS

4.1 Characterization and cytocompatibility of the CD-HA 2%Sr scaffold

The hASCs grown on the CD-HA 2%Sr scaffold (i) and TCPS (ii) as control, were used to analyse scaffold cytocompatibility. Metabolic activity, Live/Dead, cytoskeleton architecture and ECM gene expression analyses were carried out in the two experimental groups at different time points as reported below.

4.1.1 Scanning electron microscopy characterization of the CD-HA 2%Sr scaffold

The microstructure and morphology of CD-HA 2%Sr scaffolds without and with hASCs grown on them for up to 14 days were analysed using a SEM (Figure 2). Nanostructured calcium-deficient hydroxyapatite substituted with strontium shows a highly granular structure under observation at a higher magnification (80–4.00KX) (Figure 2, A-F). HASCs grown on the scaffold showed normal cell morphology, exhibiting pseudopodium-like structures, which connect them to the biomaterial surface (Figure 2, E-F).

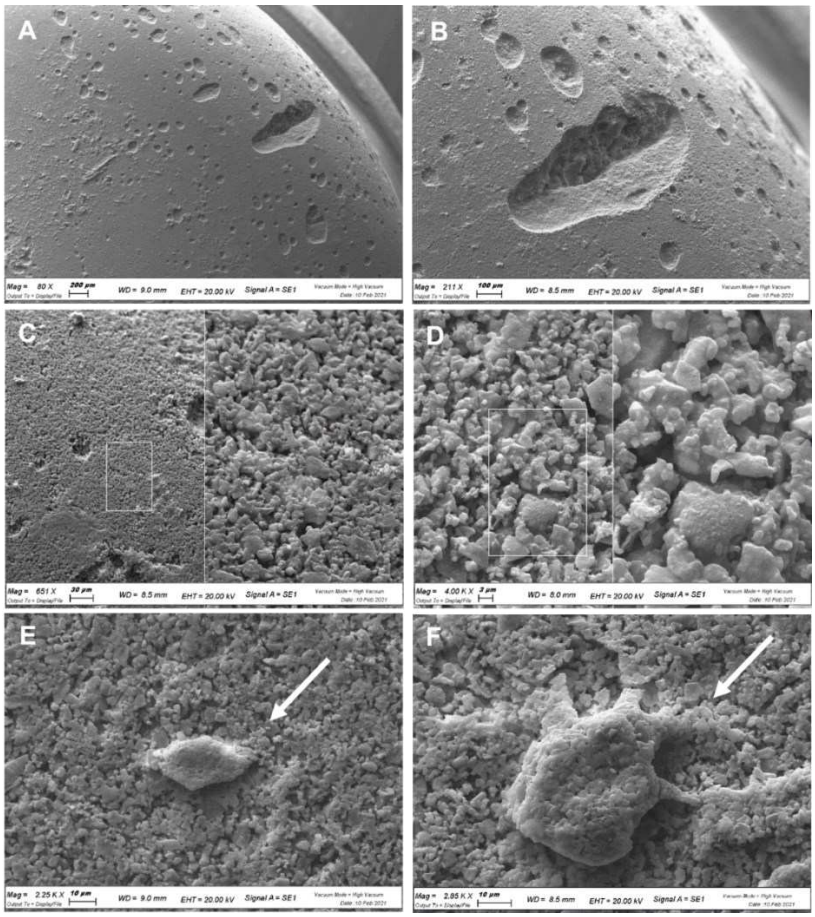

Figure 2. Scanning electron microscopy analysis of CD-HA 2%Sr scaffold. The biomaterial consists of a nanostructured calcium-deficient hydroxyapatite substituted with strontium. The structure of scaffold was observed at different magnification, Scale bar: 200 µm, 80X (A); Scale bar: 100 µm, 211X (B); Scale bar: 200 µm, 651X (C); Scale bar: 3 µm, 4.00K X (D), respectively. HASCs (white arrows) on the substrate exhibited cytoplasmic bridges, with a normal morphology; Scale bar 10 µm; 2.25K X (E); Scale bar 10 µm; 2.85K X (E), respectively.

4.1.2. Metabolic activity of hASCs grown on the CD-HA 2%Sr scaffold.

Alamar Blue assay was carried out to analyse the effects of the scaffold on hASCs cells viability. Cell metabolic activity at each time point was converted into the number of viable cells by calculating the interpolated X value of the hASCs calibration curve. Results showed an increase in terms of cell numbers for hASCs grown on the CD-HA 2%Sr scaffold and on TCPS, up to day 7. At day 1 and 2, there were no significant differences between the two experimental groups (Figure 3; $p>0.05$). Contrariwise, there are statistical differences in hASCs grown on the CD-HA 2%Sr scaffold compared to

hASCs grown on TCPS at day 7 (Figure 3; $p<0.05$). Nevertheless, CD-HA 2%Sr scaffold does induce hASCs cell growth and did not cause any cytotoxicity.

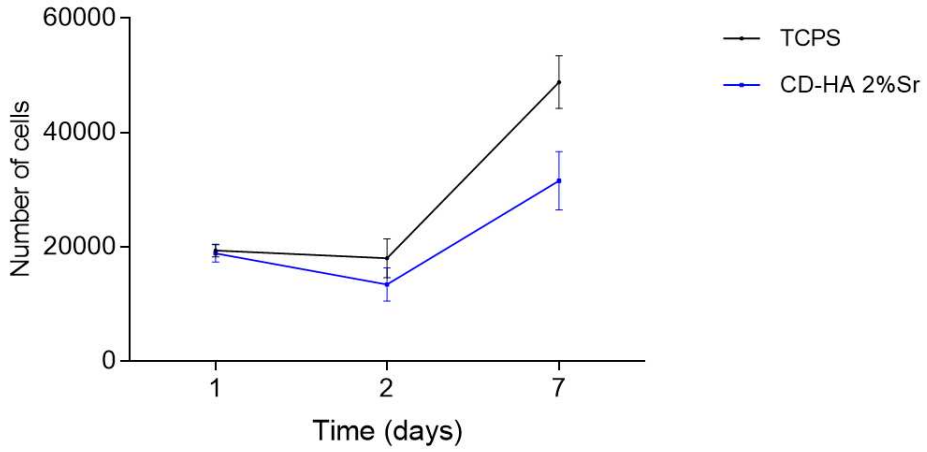

Figure 3. hASCs metabolic activity measured by Alamar Blue assay at days 1, 2, 7 of cell culture. Graph shows increasing number of hASCs grown on CD-HA 2%Sr scaffold and on TCPS up to day 7. Significant differences were revealed between CD-HA 2%Sr scaffold and TCPS at day 7 ($p<0.05$).

4.1.3. Live/Dead analysis of hASCs grown on the CD-HA 2%Sr scaffold.

Live /Dead assay was used to analyse cell viability for hASCs grown on the scaffold and in contact with it, and on TCPS, as a control, at days 3, 6 and 14. Cyto-dye, a green fluorescent dye, and propidium iodide, a red fluorescent dye, were used to stain live and dead cells, respectively. At each experimental time point, conducted on hASCs grown in contact with the scaffold, digital images showed the presence of live cells comparable to the control. Dead cells were not detected (Figure 4, A-L). In addition, live cells were also identified in the scaffold using confocal microscope in slices (z) of 0.5 µm at days 3, 6 and 14. The number of live cells increased during the experimental time course. Dead cells were not observed (Figure 5, A-F). Results demonstrated the cytocompatibility of the CD-HA 2%Sr scaffold.

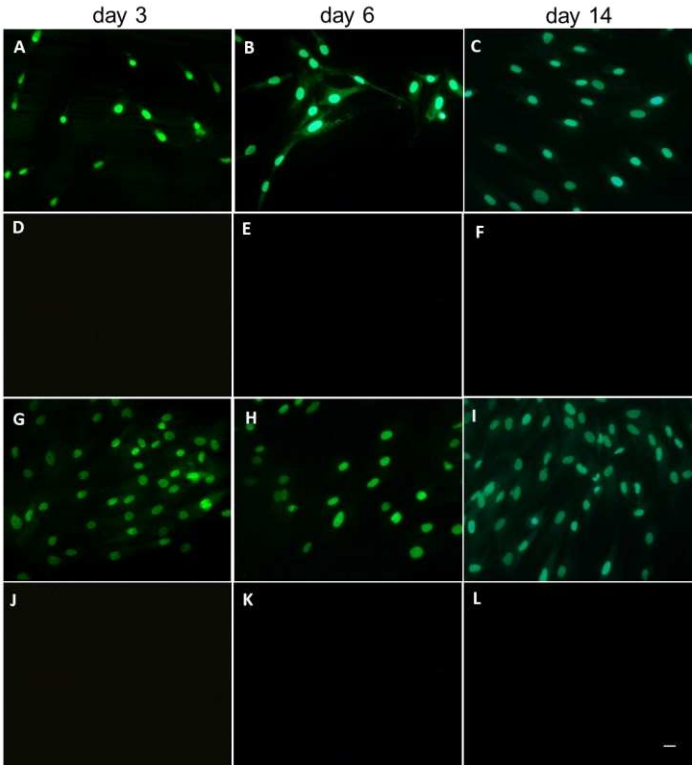

Figure 4. Cell viability analysis of hASCs in contact with CD-HA 2%Sr scaffold using Live/Dead kit. Live cells (hASCs) grown in contact with CD-HA 2%Sr at day 3 (A), 6 (B), 14 (C). Dead cells were no detected (D, E, F). Live cells (hASCs) grown on TCPS at day 3 (G), 6 (H), 14 (I). Dead cells were no detected (J, K, L). Scale bar: 100 µm.

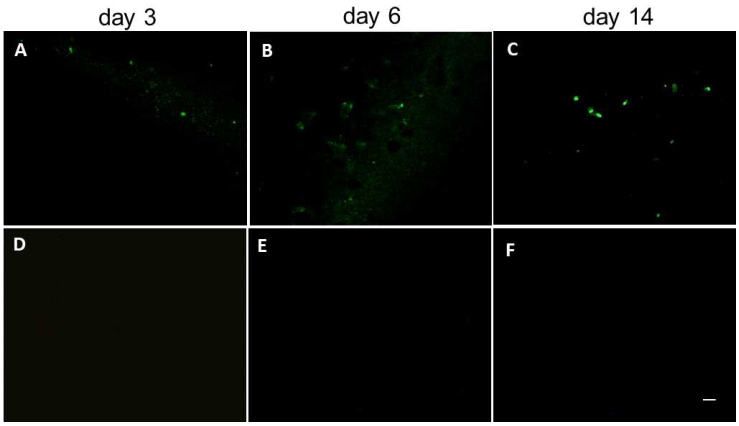

Figure 5. Cell viability analysis of hASCs on CD-HA 2%Sr scaffold using Live/Dead kit. Live cells (hASCs) grown on CD-HA 2%Sr at day 3 (A), 6 (B), 14 (C). Dead cells were no detected (D, E, F). Live cells (hASCs) grown on TCPS at day 3 (G), 6 (H), 14 (I). Dead cells were no detected (J, K, L). Z-stack images were collected at 0.5 µm slices by confocal microscopy from the bottom to the top of the cells and were merged into a single frame. Scale bar: 100 µm.

4.1.4. Cytoskeleton analysis of hASCs grown on the CD-HA 2%Sr scaffold.

The cytoskeleton architecture of hASCs grown on the CD-HA 2%Sr scaffold and on TCPS, as a control, was analysed by performing phalloidin-TRITC staining at day 14 (Figure 6). The cytoskeleton showed a well-organized structure in hASCs grown on the scaffold and on TCPS, demonstrating that the scaffold had no influence on cytoskeleton architecture up to day 14. In the digital images at 10X, 20X magnification (Figure 6, panels A-L) and 40X magnification (Figure 6, panels M-Q), actin filaments appear unaltered, confirming cytocompatibility for the CD-HA 2%Sr scaffold.

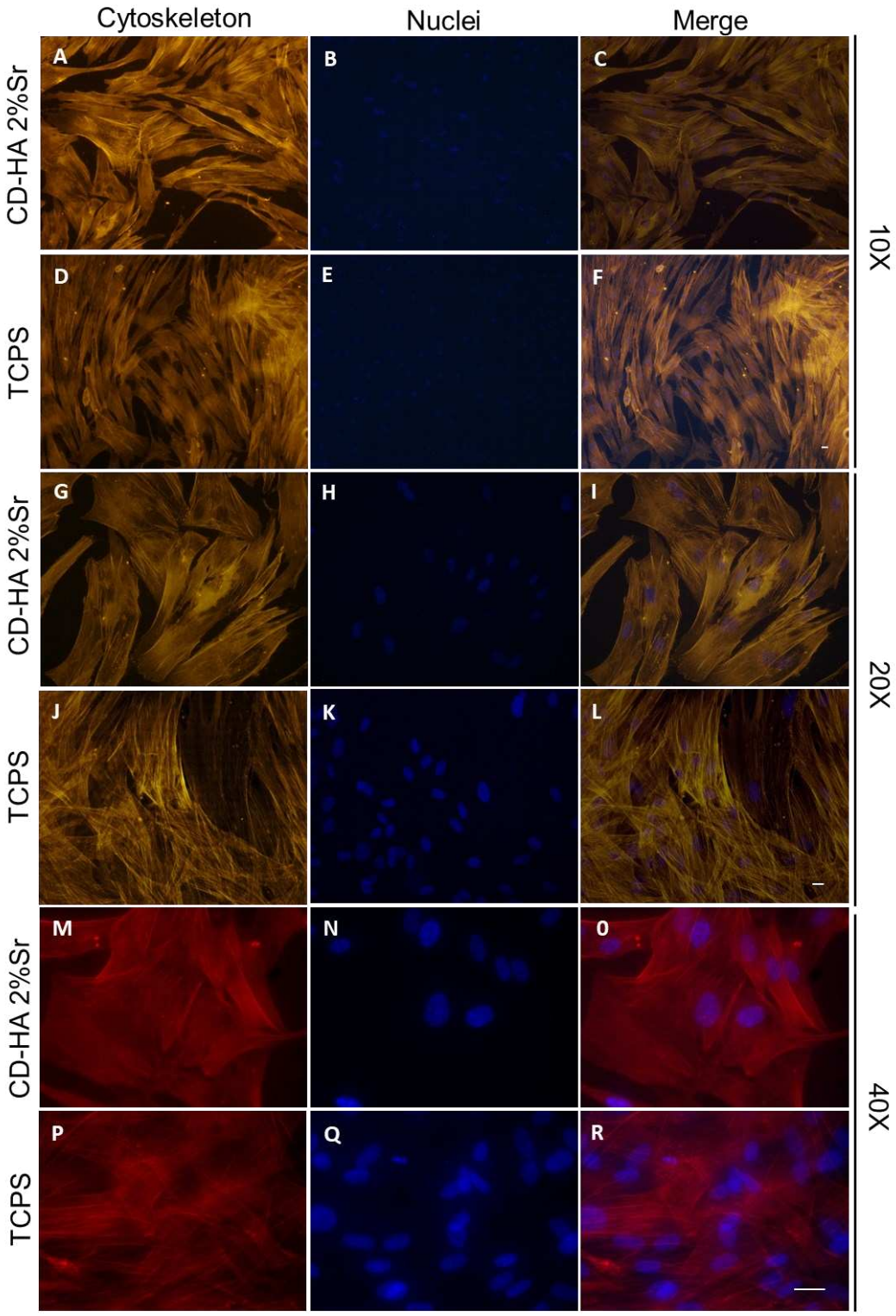

Figure 6. Cytoskeleton analysis by Phalloidin tetramethyl-rhodamine-isothiocyanate (TRITC) staining of hASCs grown on CD-HA 2%Sr scaffold. Actin filaments do not show alteration in the structural organization compared to control (TCPS) at 10X (A-F), 20X (G-L), 40X (M-R) magnification. Images at 10X and 20X magnification were acquired with TE 200-E fluorescent microscope (A-L); images at 40X were acquired with Olympus Xcellence microscope (M-Q). Scale bar for each magnification: 100 µm. Cellular nuclei were stained with 0.5 mg/mL DAPI (B-E-H-K-N-Q).

4.1.5. Extracellular matrix and adhesion molecules genes modulated by CD-HA 2%Sr scaffold in hASCs.

The ECM and adhesion molecules gene expression profiles were investigated using PCR array technology in hASCs cultured on the CD-HA 2%Sr scaffold and TCPS in order to evaluate scaffold cytocompatibility. Analyses were carried out at day 3, 6 and 14. At day 3, a total of 27 differential expressed genes, including 9 up-regulated genes (>1 $\log_2$ fold change; $p<0.05$; red) and 18 down-regulated genes (<1 $\log_2$ fold change; $p<0.05$; green), were identified in hASCs grown on scaffolds compared to the control. Results of the experimental replicates showed that the scaffold positively modulated Integrin Subunit Beta 3 (*ITGB3*), Intercellular Adhesion Molecule 1 (*ICAM1*), Collagen Type XV alpha 1 (*COL15A1*), Integrin Subunit Alpha 2 (*ITGA2*), Hyaluronan Synthase 1 (*HAS1*) genes that encode for cell adhesion molecules and Matrix metallopeptidase 1 (*MMP1*), Matrix metallopeptidase 3 (*MMP3*), ADAM Metallopeptidase with Thrombospondin Type 1 Motif 13 (*ADAMTS13*), Matrix metallopeptidase 11 (*MMP11*) genes which translate extracellular matrix molecules. Furthermore, the CD-HA 2% Sr scaffold negatively modulated extracellular molecule genes as well as Collagen Type XI alpha 1 (*COL11A1*), Secreted Protein Acidic And Cysteine Rich (*SPARC*), Collagen Type I alpha 1 (*COL1A1*), Collagen Type VIII alpha 1 (*COL8A1*), C-Type Lectin Domain Family 3 Member B (*CLEC3B*), Collagen Type IV alpha 2 (*COL4A2*), Collagen Type V alpha 1 (*COL5A1*), Connective Tissue Growth Factor (*CTGF*), Fibronectin 1 (*FN1*), Thrombospondin 1 (*THBS1*), Collagen Type XII alpha 1 (*COL12A1*), Laminin Subunit Beta 1 (*LAMB1*), Collagen Type VI alpha 1 (*COL6A1*) and cell adhesion molecule genes such as Integrin Subunit Alpha 6 (*ITGA6*) Integrin Subunit Alpha 4 (*ITGA4*), Integrin Subunit Alpha 1 (*ITGA1*), Integrin Subunit Alpha 7 (*ITGA7*) and Integrin Subunit Alpha V (*ITGAV*) (Figure 7, Table 3).

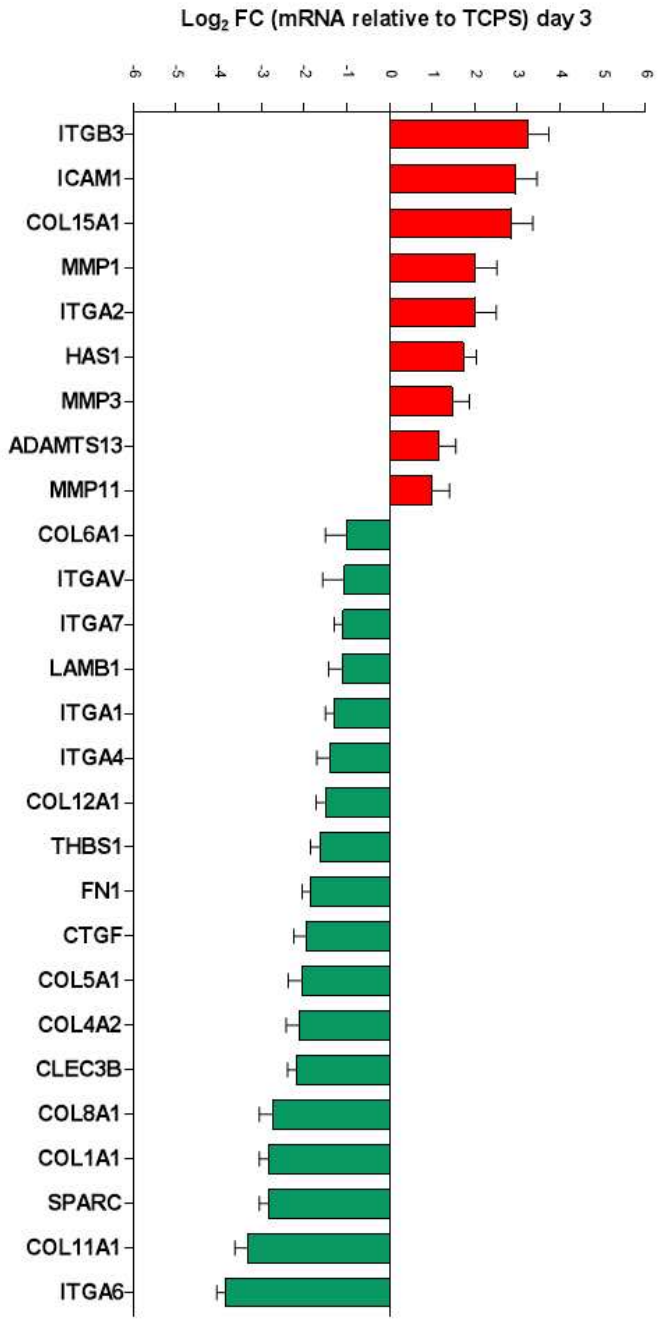

Figure 7. PCR Array results of ECM gene expression at day 3. 27 differentially expressed genes, including up-regulated genes (>1 log_2 fold change; $p<0.05$; red) and 18 down-regulated genes (<1 log_2 fold change; $p<0.05$; green), were identified in hASCs grown on scaffold compared with control.

Table 3. List of extracellular matrix genes found to be up-regulated and down-regulated in hASCs grown on the scaffold at day 3

Up-regulated genes			Down-regulated genes		
Number	Gene	Mean Log_2 FC	Number	Gene	Mean Log_2 FC
1	*ITGB3*	+3.24	1	*ITGA6*	-3.84
2	*ICAM1*	+2.96	2	*COL11A1*	-3.32
3	*COL15A1*	+2.86	3	*SPARC*	-2.84
4	*MMP1*	+2.02	4	*COL1A1*	-2.84
5	*ITGA2*	+2.01	5	*COL8A1*	-2.74
6	*HAS1*	+1.74	6	*CLEC3B*	-2.18
7	*MMP3*	+1.48	7	*COL4A2*	-2.12
8	*ADAMTS13*	+1.16	8	*COL5A1*	-2.06
9	*MMP11*	+1.01	9	*CTGF*	-1.94
			10	*FN1*	-1.84
			11	*THSB1*	-1.64
			12	*COL12A1*	-1.51
			13	*ITGA4*	-1.40
			14	*ITGA1*	-1.29
			15	*LAMB1*	-1.12
			16	*ITGA7*	-1.09
			17	*ITGAV*	-1.06
			18	*COL6A1*	-1.00

ADAM Metallopeptidase With Thrombospondin Type 1 Motif 13 (*ADAMTS13*); C-Type Lectin Domain Family 3 Member B (*CLEC3B*); Collagen Type I alpha 1 (*COL1A1*); Collagen Type IV alpha 2 (*COL4A2*); Collagen Type V alpha 1 (*COL5A1*); Collagen Type VI alpha 1 (*COL6A1*); Collagen Type VIII alpha 1 (*COL8A1*); Collagen Type XI alpha 1 (*COL11A1*); Collagen Type XII alpha 1 (*COL12A1*); Collagen Type XV alpha 1 (*COL15A1*); Connective Tissue Growth Factor (*CTGF*); Fibronectin 1 (*FN1*); Hyaluronan Synthase 1 (*HAS1*); Intercellular Adhesion Molecule 1 (*ICAM1*); Integrin Subunit Alpha 1, 2, 4, 6, 7, V (*ITGA1*, *ITGA2*, *ITGA4*, *ITGA6*, *ITGA7*, *ITGAV*); Integrin Subunit Beta 3 (*ITGB3*); Laminin Subunit Beta 1 (*LAMB1*); Matrix metallopeptidase 1, 3, 11 (*MMP1*, *MMP3*, *MMP11*); Secreted Protein Acidic And Cysteine Rich (*SPARC*); Thrombospondin 1 (*THBS1*).

At day 6, hASCs showed a total of 28 differentially expressed genes, including 12 up-regulated and 16 down-regulated genes. Specifically, Selectin L (*SELL*), Platelet And Endothelial Cell Adhesion Molecule 1 (*PECAM1*), *MMP3*, *ICAM1*, *ITGB3*, *COL15A1*, *MMP11*, *ITGA2*, *MMP1*, Collagen Type VII alpha 1 (*COL7A1*), Matrix metallopeptidase 16 (*MMP16*) genes resulted up-expressed in the presence of scaffolds, compared to TCPS, whereas *SPARC*, *COL8A1*, *COL1A1*, *ITGA4*, *COL5A1*, *COL4A2*, Secreted Phosphoprotein 1 (*SPP1*), Extracellular Matrix Protein 1 (*ECM1*), Integrin Subunit Alpha 3 (*ITGA3*), *FN1*, *CLEC3B*, *THBS1*, *COL12A1*, *COL11A1*, Laminin Subunit Beta 3 (*LAMB3*), *ITGAV* resulted down-expressed (Figure 8, Table 4).

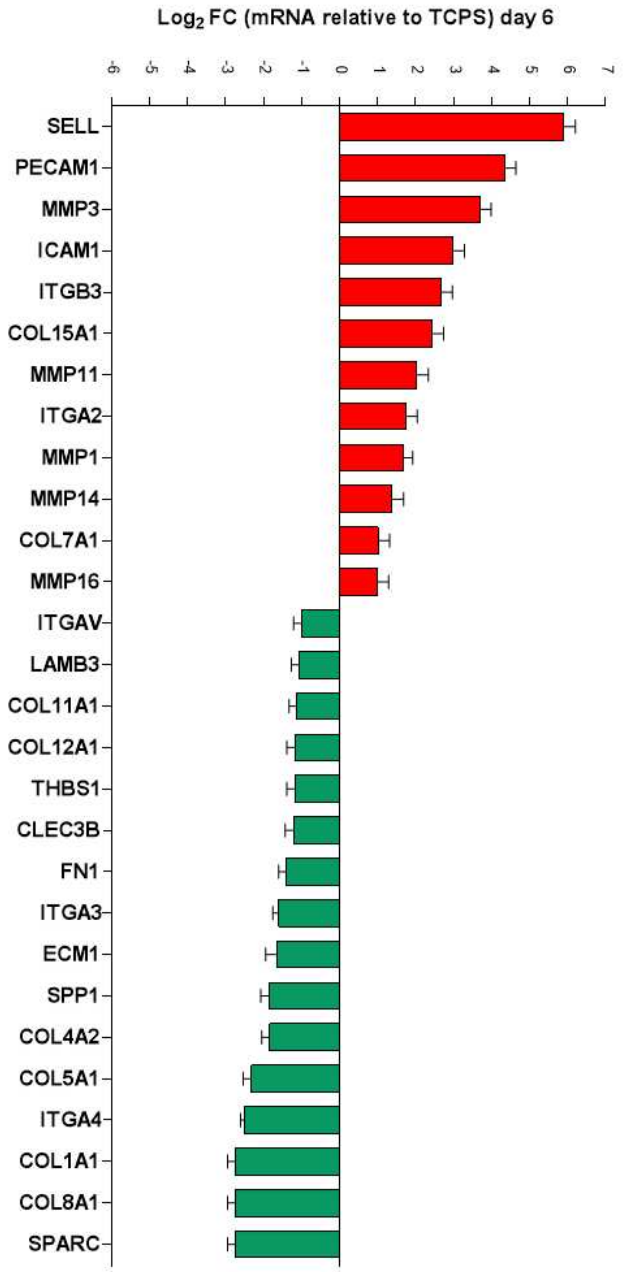

Figure 8. PCR Array results of ECM gene expression at day 6. 28 differentially expressed genes, including 12 up-regulated genes (>1 log_2 fold change; $p<0.05$; red) and 16 down-regulated genes (<1 log_2 fold change; $p<0.05$; green), were identified in hASCs grown on scaffold compared with control.

Table 4. List of extracellular matrix genes found to be up-regulated and down-regulated in hASCs grown on the scaffold at day 6

Up-regulated genes			Down-regulated genes		
Number	Gene	Mean Log_2 FC	Number	Gene	Mean Log_2 FC
1	*SELL*	+5.91	1	*SPARC*	-2.74
2	*PECAM1*	+4.84	2	*COL8A1*	-2.74
3	*MMP3*	+3.69	3	*COL1A1*	-2.74
4	*ICAM1*	+2.99	4	*ITGA4*	-2.40
5	*ITGB3*	+2.67	5	*COL5A1*	-2.32
6	*COL15A1*	+2.44	6	*COL4A2*	-1.84
7	*MMP11*	+2.04	7	*SPP1*	-1.79
8	*ITGA2*	+1.75	8	*ECM1*	-1.64
9	*MMP1*	+1.71	9	*ITGA3*	-1.60
10	*MMP14*	+1.39	10	*FN1*	-1.40
11	*COL7A1*	+1.02	11	*CLEC3B*	-1.22
12	*MMP16*	+1.00	12	*THBS1*	-1.18
			13	*COL12A1*	-1.18
			14	*COL11A1*	-1.12
			15	*LAMB3*	-1.06
			16	*ITGAV*	-1.00

C-Type Lectin Domain Family 3 Member B (*CLEC3B*); Collagen Type I alpha 1 (*COL1A1*); Collagen Type IV alpha 2 (*COL4A2*); Collagen Type V alpha 1 (*COL5A1*); Collagen Type VII alpha 1 (*COL7A1*); Collagen Type VIII alpha 1 (*COL8A1*); Collagen Type XI alpha 1 (*COL11A1*); Collagen Type XII alpha 1 (*COL12A1*); Collagen Type XV alpha 1 (*COL15A1*); Extracellular Matrix Protein 1 (*ECM1*); Fibronectin 1 (*FN1*); Intercellular Adhesion Molecule 1 (*ICAM1*); Integrin Subunit Alpha 2, 3, 4, V (*ITGA2*, *ITGA3*, *ITGA4*, *ITGAV*); Integrin Subunit Beta 3 (*ITGB3*); Laminin Subunit Beta 3 (*LAMB3*); Matrix metallopeptidase 1, 3, 11, 14, 16 (*MMP1*, *MMP3*, *MMP11*, *MMP14*, *MMP16*); Platelet And Endothelial Cell Adhesion Molecule 1 (*PECAM1*); Selectin L (*SELL*); Secreted Protein Acidic And Cysteine Rich (*SPARC*); Secreted Phosphoprotein 1 (*SPP1*); Thrombospondin 1 (*THBS1*).

At day 14, genes encoding cell adhesion molecules including Cadherin 1 (*CDH1*), Integrin Subunit Alpha 8 (*ITGA8*), Catenin Delta 1 (*CTNND1*), *ITGA6*, *ITGA4*, Catenin Beta 1 (*CTNNB1*), *ITGA2*, *ITGA3*, Vascular Cell Adhesion Molecule 1 (*VCAM1*), and genes encoding extracellular matrix molecules such as ADAM Metallopeptidase with Thrombospondin Type 1 Motif 8 (*ADAMTS8*), *ADAMTS13*, *CLEC3B*, ADAM Metallopeptidase With Thrombospondin Type 1 Motif 1 (A*DAMTS1*), CD44 Molecule

(*CD44*), Matrix metallopeptidase 15 (*MMP15*), Anosmin 1 (*ANOS1*), *PECAM1*, Laminin Subunit Alpha 3 (*LAMA3*), Vitronectin (*VTN*), Matrix metallopeptidase 8 (*MMP8*), Collagen Type XIV alpha 1 (*COL14A1*), *LAMB3*, Thrombospondin 3 (*THBS3*), Laminin Subunit Alpha 2 (*LAMA2*), *COL11A1*, SPG7 Matrix AAA Peptidase Subunit, Paraplegin (*SPG7*), *COL8A1*, Tenascin C (*TNC*) and *COL15A1* resulted up-regulated in hASCs grown on the scaffolds compared to hASCs grown on TCPS. Contrariwise, genes for extracellular matrix molecules including *FN1*, Matrix metallopeptidase 2 (*MMP2*), TIMP Metallopeptidase Inhibitor 1, 2, and 3 (*TIMP1*, *TIMP2*, *TIMP3*), Thrombospondin 2 (*THBS2*), Collagen Type VI alpha 2 (*COL6A2*), and for cell adhesion molecules such as Integrin Subunit Beta 1 (*ITGB1*), Integrin Subunit Alpha 5 (*ITGA5*), were negatively regulated by the scaffold (Figure 9, Table 5).

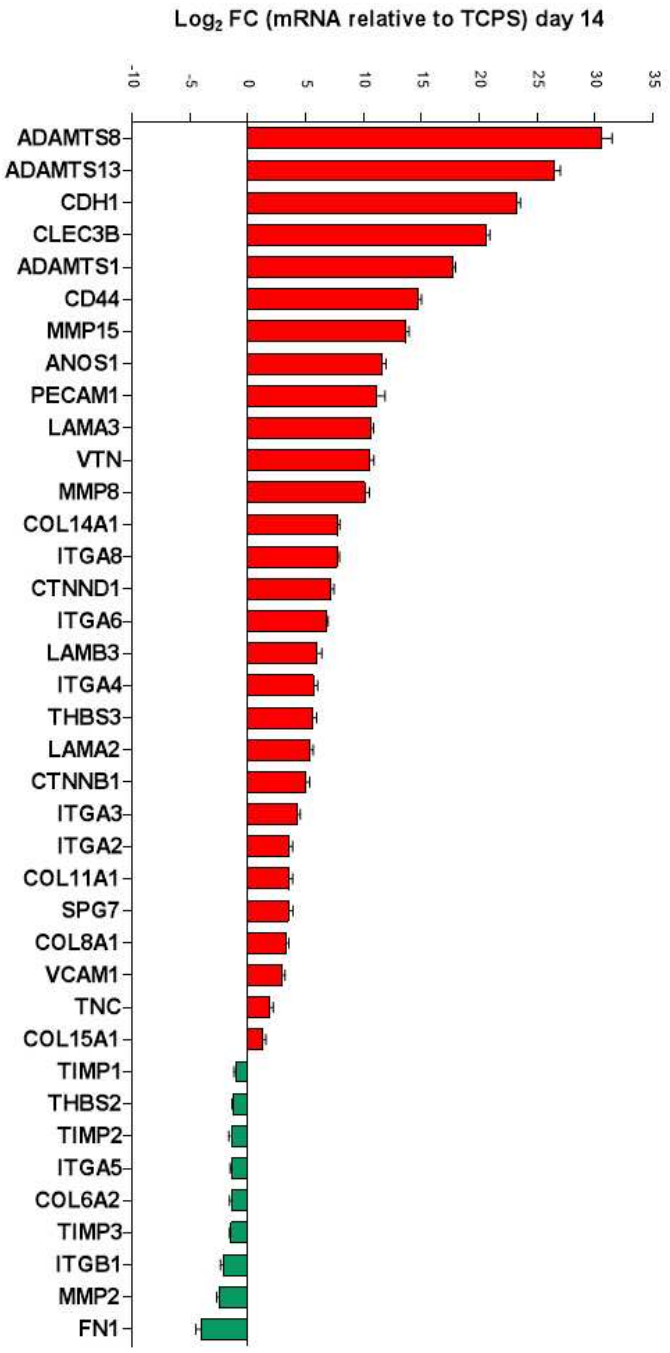

Figure 9. PCR Array results of ECM gene expression at day 14. 38 differentially expressed genes, including 29 up-regulated genes (>1 log_2 fold change; $p<0.05$; red) and 9 down-regulated genes (<1 log_2 fold change; $p<0.05$; green), were identified in hASCs grown on scaffold compared with control.

Table 5. List of extracellular matrix genes found to be up-regulated and down-regulated in hASCs grown on the scaffold at day 14

Up-regulated genes			Down-regulated genes		
Number	Gene	Mean Log_2 FC	Number	Gene	Mean Log_2 FC
1	*ADAMTS8*	+30.15	1	*FN1*	-4.06
2	*ADAMTS13*	+26.62	2	*MMP2*	-2.47
3	*CDH1*	+23.29	3	*ITGB1*	-2.12
4	*CLEC3B*	+20.59	4	*TIMP3*	-1.47
5	*ADAMTS1*	+17.77	5	*COL6A2*	-1.43
6	*CD44*	+14.83	6	*ITGA5*	-1.40
7	*MMP15*	+13.61	7	*TIMP2*	-1.32
8	*ANOS1*	+11.33	8	*THBS2*	-1.25
9	*PECAM1*	+11.05	9	*TIMP1*	-1.06
10	*LAMA3*	+10.70			
11	*VTN*	+10.54			
12	*MMP8*	+10.14			
13	*COL14A1*	+7.79			
14	*ITGA8*	+7.64			
15	*CTNND1*	+7.18			
16	*ITGA6*	+6.74			
17	*LAMB3*	+6.02			
18	*ITGA4*	+5.81			
19	*THBS3*	+5.59			
20	*LAMA2*	+5.38			
21	*CTNNB1*	+4.97			
22	*ITGA3*	+4.35			
23	*ITGA2*	+3.63			
24	*COL11A1*	+3.60			
25	*SPG7*	+3.55			
26	*COL8A1*	+3.36			
27	*VCAM1*	+2.95			
28	*TNC*	+1.93			
29	*COL15A1*	+1.29			

ADAM Metallopeptidase With Thrombospondin Type 1 Motif 1 (*ADAMTS1*); ADAM Metallopeptidase With Thrombospondin Type 1 Motif 8 (*ADAMTS8*); ADAM Metallopeptidase With Thrombospondin Type 1 Motif 13 (*ADAMTS13*); Anosmin 1 (*ANOS1*); CD44 Molecule (*CD44*); Cadherin 1 (*CDH1*); C-Type Lectin Domain Family 3 Member B (*CLEC3B*); Collagen Type VI alpha 2 (*COL6A2*); Collagen Type VIII alpha 1 (*COL8A1*); Collagen Type XI alpha 1 (*COL11A1*); Collagen Type XIV alpha 1 (*COL14A1*); Collagen Type XV alpha 1 (*COL15A1*); Catenin Beta 1 (*CTNNB1*); Catenin Delta 1 (*CTNND1*); Fibronectin 1 (*FN1*); Integrin Subunit Alpha 2, 3, 4, 5, 6, 8 (*ITGA2*, *ITGA3*, *ITGA4*, *ITGA5*, *ITGA6*, *ITGA8*); Integrin Subunit Beta 1 (*ITGB1*); Laminin Subunit Alpha 2 and 3 (*LAMA2* and *LAMA3*); Laminin Subunit Beta 3 (*LAMB3*); Matrix metallopeptidase 2, 8, 15 (*MMP2*, *MMP8*, *MMP15*); Platelet And Endothelial Cell Adhesion Molecule 1 (*PECAM1*); SPG7 Matrix AAA Peptidase Subunit, Paraplegin (*SPG7*); Thrombospondin 2

and 3 (*THBS2* and *THBS3*); TIMP Metallopeptidase Inhibitor 1, 2, 3 (*TIMP1*, *TIMP2*, *TIMP3*); Tenascin C (*TNC*); Vascular Cell Adhesion Molecule 1 (*VCAM1*); Vitronectin (*VTN*).

4.2. Osteoinductivity properties of the CD-HA 2%Sr scaffold

In the second phase of the study, the osteoinductivity properties of the CD-HA 2%Sr scaffold were assessed employing an *in vitro* study model constituted by hASCs. Matrix mineralization, osteocalcin protein expression and osteogenic genes expression were investigated in hASCs grown on the scaffold up to day 14.

4.2.1. Mineral matrix deposition of hASCs grown on CD-HA 2%Sr scaffold

Alizarin Red staining was used to evaluate the mineralized matrix using hASCs cultures grown on the CD-HA 2%Sr scaffold and on TCPS used as control. To this end, cell cultures for two experimental groups were stained with alizarin red and imaged using a bright-field microscope. Digital images show that CD-HA 2%Sr scaffold promotes mineral matrix deposition differently from TCPS (Figure 10, Panels A-F). Afterwards, alizarin red staining was eluted to perform optical density measurements. Results showed an increased calcified matrix in hASCs grown on the CD-HA 2%Sr scaffold compared to TCPS ($p < 0.0001$; Figure 10, Panel G) at day 14.

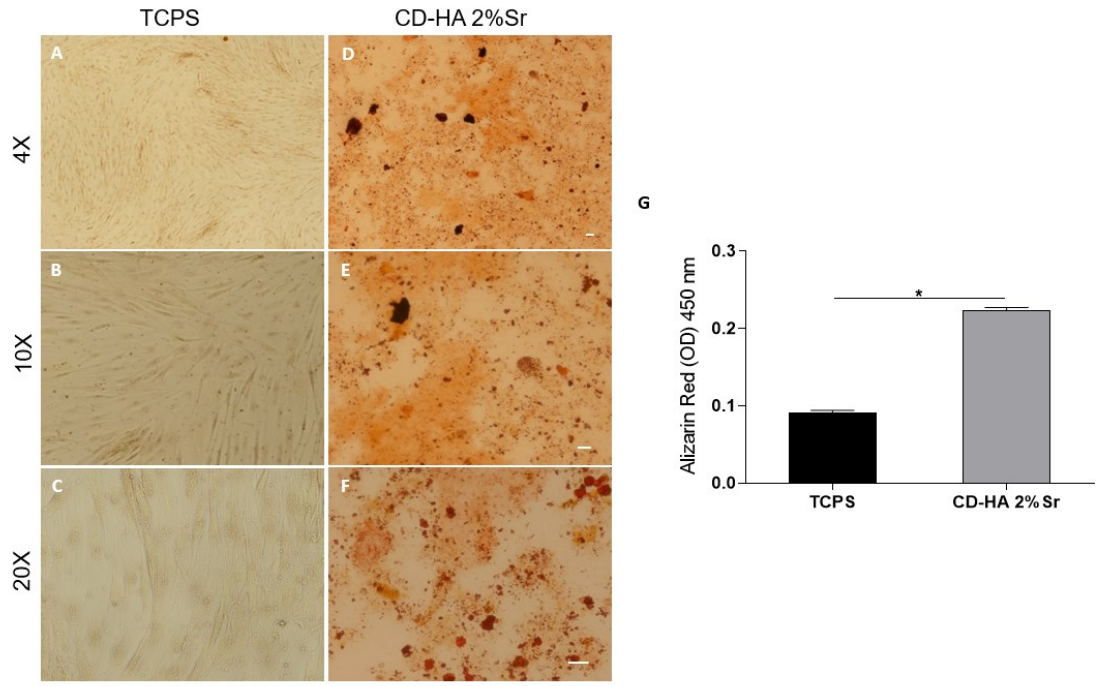

Figure 10. Mineral matrix deposition analysis at day 14. Alizarin red staining in hASCs grown on TCPS at 4X (A), 10X (B), and 20X (C), respectively. Alizarin red staining in hASCs grown on CD-HA 2%Sr scaffold at 4X (A), 10X (B), and 20X (C), respectively. Scale bar for each magnification: 100 µm. Quantification of Alizarin Red staining through spectrophotometric analysis at 450 nm wavelength ($p < 0.0001$).

4.2.2. Osteocalcin protein expression in hASCs grown on the CD-HA 2%Sr scaffold.

OCN protein expression in hASCs grown on the CD-HA 2%Sr scaffold and on TCPS up to day 14 were analysed using ELISA test. In hASCs grown on the CD-HA 2%Sr the assay revealed 38,25 ng/µg of OCN and 17,95 ng/µg of OCN in TCPS. Data show a statistical increase of OCN protein expression in hASCs grown on the scaffold compared to cells grown on TCPS ($p<0.0001$; Figure 11).

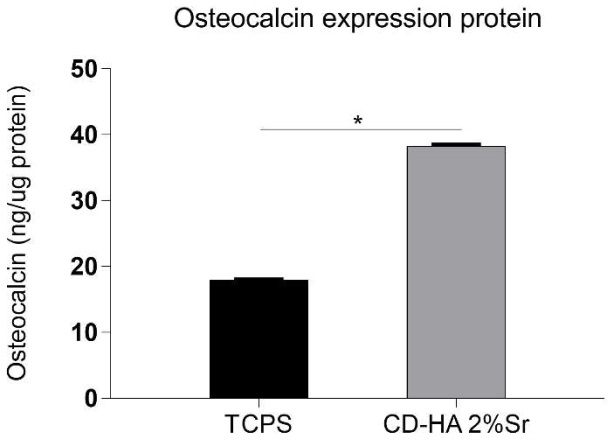

Figure 11. Osteocalcin protein expression at day 14. Osteocalcin protein expression was quantified using ELISA test in hASCs grown on CD-HA 2%Sr scaffold and on TCPS at day 14 (<0.0001).

4.2.3. Osteogenic genes modulated by the CD-HA 2%Sr scaffold in hASCs.

In this study osteogenesis RT^2 Profiler PCR Array was used to investigate differentially expressed genes in hASCs grown on CD-HA 2%Sr scaffolds at days 3, 6 and 14. Results of experimental replicates obtained at day 3 revealed the ability of the scaffold to up-regulate (>1 $\log_2$ fold change; $p<0.05$; red) different genes involved in skeletal development including Bone Morphogenetic Proteins 2 (*BMP2*), GLI family zinc finger 1 (*GLI1*), Runt-related Transcription Factor 2 (*RUNX2*), Bone Gamma-Carboxyglutamate Protein (*BGLAP*), Fibroblast Growth Factor 2 (*FGF2*), in cell adhesion molecules such as Colony Stimulating Factor 2 and 3 (*CSF2* and *CSF3*), Vascular Endothelial Growth Factor A (*VEGFA*), Insulin Growth Factor 1 (*IGF1*), *ICAM1*, *ITGA2*, and in bone metabolism with *COL15A1*, and Matrix metallopeptidase 10 (*MMP10*) as shown in (Figure 12, Table 6). Contrariwise, at the same time point, the genes which resulted down-regulated (<1 log2 fold change; $p<0.05$; green) were Fibroblast Growth Factor 1 (*FGF1*), Noggin (*NOG*), *COL1A1*, Bone Morphogenetic Proteins 4 (*BMP4*),

Cartilage Oligomeric Matrix Protein (*COMP*), *COL5A1*, Alkaline Phosphatase (*ALPL*), *FN1*, CD36 molecule (*CD36*), *ITGA1*, *SPP1*, Serpin Family H Member 1 (*SERPINH1*), Collagen Type III alpha 1 (*COL3A1*), *ITGA3*, Biglycan (*BGN*), Collagen Type I alpha 2 (*COL1A2*), Bone Morphogenetic Proteins 1 (*BMP1*), Cadherin 11, type 2 (*CDH11*), Transforming Growth Factor Beta Receptor 2 (*TGFBR2*), Fibroblast Growth Factor Receptor 2 (*FGFR2*) and *ITGB1* (Figure 12, Table 6).

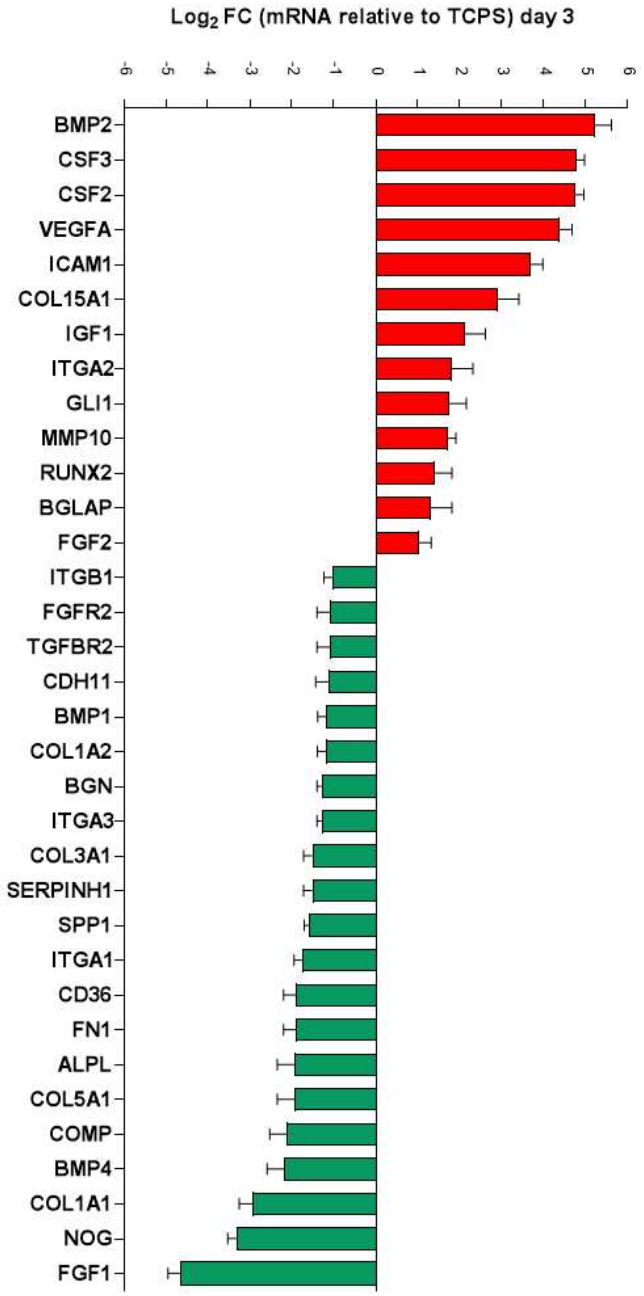

Figure 12. PCR Array results of human osteogenesis gene expression at day 3. 34 differentially expressed genes, including 13 up-regulated genes (>1 log_2 fold change; $p<0.05$; red) and 21 down-regulated genes (<1 log_2 fold change; $p<0.05$; green), were identified in hASCs grown on scaffold compared with control.

Table 6. List of osteogenic genes found to be up-regulated and down-regulated in hASCs grown on the scaffold at day 3

Up-regulated genes			Down-regulated genes		
Number	Gene	Mean Log_2 FC	Number	Gene	Mean Log_2 FC
1	*BMP2*	+5.22	1	*FGF1*	-4.64
2	*CSF3*	+4.78	2	*NOG*	-3.32
3	*CSF2*	+4.76	3	*COL1A1*	-2.94
4	*VEGFA*	+4.38	4	*BMP4*	-2.18
5	*ICAM1*	+3.69	5	*COMP*	-2.12
6	*COL15A1*	+2.91	6	*COL5A1*	-1.94
7	*IGF1*	+2.12	7	*ALPL*	-1.94
8	*ITGA2*	+1.82	8	*FN1*	-1.89
9	*GLI1*	+1.76	9	*CD36*	-1.89
10	*MMP10*	+1.72	10	*ITGA1*	-1.74
11	*RUNX2*	+1.42	11	*SPP1*	-1.60
12	*BGLAP*	+1.32	12	*SERPINH1*	-1.51
13	*FGF2*	+1.03	13	*COL3A1*	-1.51
			14	*ITGA3*	-1.29
			15	*BGN*	-1.29
			16	*COL1A2*	-1.18
			17	*BMP1*	-1.18
			18	*CDH11*	-1.12
			19	*TGFBR2*	-1.09
			20	*FGFR2*	-1.09
			21	*ITGB1*	-1.03

Alkaline Phosphatase (*ALPL*); Bone Gamma-Carboxyglutamate Protein (*BGLAP*); Biglycan (*BGN*); Bone Morphogenetic Proteins 1, 2, 4 (*BMP1*, *BMP2*, *BMP4*); CD36 molecule (*CD36*); Cadherin 11, type 2 (*CDH11*); Collagen Type I alpha 1 (*COL1A1*); Collagen Type I alpha 2 (*COL1A2*); Collagen Type III alpha 1 (*COL3A1*); Collagen Type IV alpha 1 (*COL5A1*); Collagen Type XV alpha 1 (COL15A1); Cartilage Oligomeric Matrix Protein (*COMP*); Colony Stimulating Factor 2 and 3 (*CSF2* and *CSF3*); Fibroblast Growth Factor 1 and 2 (*FGF1* and *FGF2*); Fibroblast Growth Factor Receptor 2 (*FGFR2*); Fibronectin 1 (*FN1*); GLI family zinc finger 1 (*GLI1*); Intercellular adhesion molecule 1 (*ICAM1*); Insulin Growth Factor 1 (*IGF1*); Integrin Subunit Alpha 1, 2, 3 (*ITGA1*, *ITGA2*, *ITGA3*); Integrin Subunit Beta 1 (*ITGB1*); Matrix metallopeptidase 10 (*MMP10*); Noggin (*NOG*); Runt-related Transcription Factor 2 (*RUNX2*); Serpin Family H Member 1 (*SERPINH1*); Secreted Phosphoprotein 1 (*SPP1*); Transforming Growth Factor Beta Receptor 2 (*TGFBR2*); Vascular Endothelial Growth Factor A (*VEGFA*).

At day 6, the majority of genes which were up-regulated from the scaffold in hASCs were involved in skeletal development such as TNF Superfamily Member 11 (*TNFSF11*), *BMP2*, Bone Morphogenetic Proteins 7 (*BMP7*), Sp7 Transcription Factor (*SP7*), Transforming Growth Factor Beta 2 (*TGFB2*), Vitamin D Receptor (*VDR*), Transforming Growth Factor Beta Receptor 1 (*TGFBR1*), *FGF2*, *BMP4*, *RUNX2* and Bone Morphogenetic Protein Receptor Type 1B (*BMPR1B*). Other up-regulated genes encode for cell adhesion molecules including *CSF3*, *VEGFA*, *ICAM1*, *ITGA2*, Vascular Endothelial Growth Factor B (*VEGFB*), SRY-Box Transcription Factor 9 (*SOX9*), Epidermal Growth Factor Receptor (*EGFR*) and bone mineral metabolism such as *COL15A1*. At day 6, the CD-HA 2% Sr scaffold negatively modulated more genes involved in extracellular matrix deposition molecules such as *COMP*, *COL1A1*, *COL3A1*, *COL5A1*, Actin Beta (*ACTB*), *COL1A2*, *SERPINH1*, *FN1*, Hypoxanthine Phosphoribosyltransferase 1 (*HPRT1*), than genes involved in skeletal development like *SPP1*, Twist Family BHLH Transcription Factor 1 (*TWIST1*), Bone Morphogenetic Proteins 6 (*BMP6*), and *BMP1* (Figure 13, Table 7).

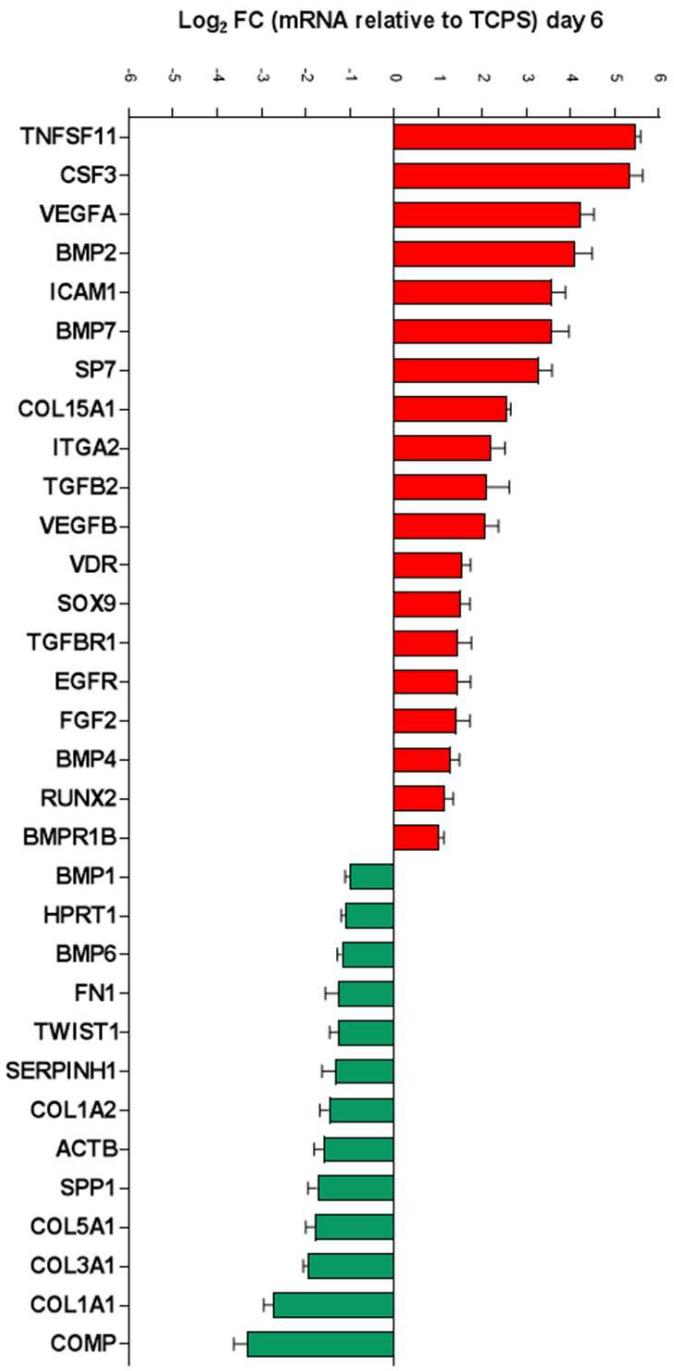

Figure 13. PCR Array results of human osteogenesis gene expression at day 6. 32 differentially expressed genes, including 19 up-regulated genes (>1 $\log_2$ fold change; $p<0.05$; red) and 13 down-regulated genes (<1 $\log_2$ fold change; $p<0.05$; green), were identified in hASCs grown on scaffold compared with control.

Table 7. List of osteogenic genes found to be up-regulated and down-regulated in hASCs grown on the scaffold at day 6

Up-regulated genes			Down-regulated genes		
Number	Gene	Mean Log_2 FC	Number	Gene	Mean Log_2 FC
1	*TNFSF11*	+5.48	1	*COMP*	-3.32
2	*CSF3*	+5.34	2	*COL1A1*	-2.74
3	*VEGFA*	+4.23	3	*COL3A1*	-1.94
4	*BMP2*	+4.09	4	*COL5A1*	-1.79
5	*ICAM1*	+3.58	5	*SPP1*	-1.74
6	*BMP7*	+3.57	6	*ACTB*	-1.60
7	*SP7*	+3.28	7	*COL1A2*	-1.47
8	*COL15A1*	+2.55	8	*SERPINH1*	-1.32
9	*ITGA2*	+2.22	9	*TWIST1*	-1.25
10	*TGFB2*	+2.12	10	*FN1*	-1.25
11	*VEGFB*	+2.07	11	*BMP6*	-1.18
12	*VDR*	+1.54	12	*HPRT1*	-1.09
13	*SOX9*	+1.52	13	*BMP1*	-1.00
14	*TGFBR1*	+1.46			
15	*EGFR*	+1.44			
16	*FGF2*	+1.42			
17	*BMP4*	+1.29			
18	*RUNX2*	+1.15			
19	*BMPR1B*	+1.04			

Actin Beta (*ACTB*); Bone Morphogenetic Proteins 1, 2, 4, 6, 7 (*BMP1*, *BMP2*, *BMP4*, *BMP6*, *BMP7*); Bone Morphogenetic Protein Receptor Type 1B (*BMPR1B*); Collagen Type I alpha 1 (*COL1A1*); Collagen Type I alpha 2 (*COL1A2*); Collagen Type III alpha 1 (*COL3A1*); Collagen Type IV alpha 1 (*COL5A1*); Collagen Type XV alpha 1 (*COL15A1*); Cartilage Oligomeric Matrix Protein (*COMP*); Colony Stimulating Factor 3 (*CSF3*); Epidermal Growth Factor Receptor (*EGFR*); Fibroblast Growth Factor 2 (*FGF2*); Fibronectin 1 (*FN1*); Hypoxanthine Phosphoribosyl transferase 1 (*HPRT1*); Intercellular adhesion molecule 1 (*ICAM1*); Integrin Subunit Alpha 2 (*ITGA2*); Runt-related Transcription Factor 2 (*RUNX2*); Serpin Family H Member 1 (*SERPINH1*); SRY-Box Transcription Factor 9 (*SOX9*); Sp7 Transcription Factor (*SP7*); Secreted Phosphoprotein 1 (*SPP1*); Transforming Growth Factor Beta 2 (*TGFB2*); Transforming Growth Factor Beta Receptor 1 (*TGFBR1*); TNF Superfamily Member 11 (*TNFSF11*); Twist Family BHLH Transcription Factor 1 (*TWIST1*); Vitamin D Receptor (*VDR*); Vascular Endothelial Growth Factor A and B (*VEGFA* and *VEGFB*).

At day 14 *SP7*, TNF Superfamily Member 11 (*TNSF11*), *MMP10*, *GLI1*, *FGFR2*, *ALPL*, SMAD Family Member 5 (*SMAD5*), Nuclear Factor Kappa B Subunit 1 (*NFKB1*), Bone Morphogenetic Protein Receptor 2 (*BMPR2*), Fibroblast Growth Factor Receptor 1 (*FGFR1*) genes inducing skeletal development and Integrin Subunit Alpha M (*ITGAM*), *CSF3*, Epidermal Growth Factor (*EGF*), *ITGA3*, *COL14A1*, *VEGFA*, *COL15A1*, implicated in bone metabolism and cell adhesion molecules were positively regulated by CD-HA 2%Sr scaffolds. Contrariwise *COMP*, *COL3A1*, *FN1*, *COL1A2*, *COL1A1*, *BNG*, and *TGFB1* genes were negatively regulated by CD-HA 2%Sr scaffolds compared to TCPS (Figure 14, Table 8).

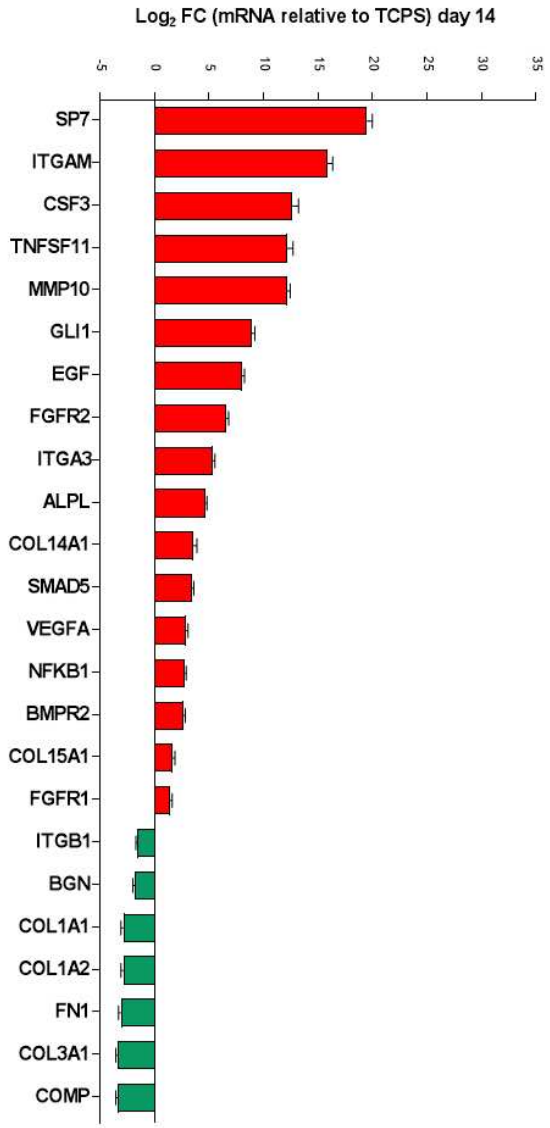

Figure 14. PCR Array results of human osteogenesis gene expression at day 14. 24 differentially expressed genes, including 17 up-regulated genes (>1 log_2 fold change; $p<0.05$; red) and 7 down-regulated genes (<1 log_2 fold change; $p<0.05$; green), were identified in hASCs grown on scaffold compared with control.

Table 8. List of osteogenic genes found to be up-regulated and down-regulated in hASCs grown on the scaffold at day 14.

Up-regulated genes			Down-regulated genes		
Number	Gene	Mean Log_2 FC	Number	Gene	Mean Log_2 FC
1	*SP7*	+19.52	1	*COMP*	-3.32
2	*ITGAM*	+15.89	2	*COL3A1*	-3.32
3	*CSF3*	+13.00	3	*FN1*	-3.06
4	*TNFSF11*	+12.25	4	*COL1A2*	-2.84
5	*MMP10*	+12.19	5	*COL1A1*	-2.84
6	*GLI1*	+8.59	6	*BNG*	-1.74
7	*EGF*	+8.09	7	*ITGB1*	-1.56
8	*FGFR2*	+6.64			
9	*ITGA3*	+5.38			
10	*ALPL*	+4.67			
11	*COL14A1*	+3.63			
12	*SMAD5*	+3.45			
13	*VEGFA*	+2.91			
14	*NFKB1*	+2.77			
15	*BMPR2*	+2.68			
16	*COL15A1*	+1.71			
17	*FGFR1*	+1.47			

Alkaline Phosphatase (*ALP*); Biglycan (*BGN*); Bone Morphogenetic Protein Receptor Type 2 (*BMPR2*); Collagen Type I alpha 1 (*COL1A1*); Collagen Type I alpha 2 (*COL1A2*); Collagen Type III alpha 1 (*COL3A1*); Collagen Type XIV alpha 1 (*COL14A1*); Collagen Type XV alpha 1 (*COL15A1*); Cartilage Oligomeric Matrix Protein (*COMP*); Colony Stimulating Factor 3 (*CSF3*); Epidermal Growth Factor (*EGF*); Fibroblast Growth Factor Receptor 1 (*FGFR1*); Fibroblast Growth Factor Receptor 2 (*FGFR2*); Fibronectin 1 (*FN1*); GLI family zinc finger 1 (*GLI1*); Integrin Subunit Alpha 3 (*ITGA3*); Integrin Subunit Alpha M (*ITGAM*); Integrin Subunit Beta 1 (*ITGB1*); Matrix metallopeptidase 10 (*MMP10*); Nuclear Factor Kappa B Subunit 1 (*NFKB1*); SMAD Family Member 5 (*SMAD5*); Sp7 Transcription Factor (*SP7*); TNF Superfamily Member 11 (*TNFSF11*); Vascular Endothelial Growth Factor A (*VEGFA*).

In summary, the scaffold strengthened the expression of genes implicated in ossification, osteoblast differentiation, and bone mineralization in hASCs during the experimental time course, whereas the modulation of genes involved in the cell adhesion process decreased over the14 days.

4.3. Cytotoxic effects analyses of the drug-linked CD-HA 2%Sr scaffolds on SAOS-eGFP cells

Anti-proliferative features of the innovative CD-HA 2%Sr-MTX and CD-HA 2%Sr-DOX drug-linked scaffolds on OS cells were investigated using different assays including on SEM analysis, viability and metabolic activity of SAOS-eGFP cells up to day 7.

4.4. Scanning electron microscopy (SEM) characterization of SAOS-eGFP cells grown on the CD-HA 2%Sr drug-linked scaffold

SEM analysis was used to investigate the structural characteristics of functionalized cements with SAOS-eGFP cells grown on them up to day 7. Images were acquired at 268-3.07KX magnification range. Similarly, to the CD-HA 2%Sr scaffold, CD-HA 2%Sr-MTX and CD-HA 2%Sr-DOX also have a highly-granular structure (Figure 15). After 7 days, the CD-HA 2%Sr scaffold surface was nearly completely covered by SAOS-eGFP cells exhibiting their natural morphology and cytoplasmic extensions in contact with the scaffold surface and with other cells (Figure 15, Panel A, B, C, D). SAOS-eGFP cells grown on CD-HA 2%Sr-MTX at up to day 7 covered the scaffold surface almost completely. However, cells showed damaged morphology compared to SAOS-eGFP cells grown on the control as shown in Figure 15, Panel E, F, G, H. Contrariwise, CD-HA 2%Sr-DOX is not covered by SAOS-eGFP cells; only a few cells with altered morphology were visible on the scaffold surface (Figure 15, Panel I, J, K, L). These results indicate that CD-HA 2%Sr-MTX and CD-HA 2%Sr-DOX scaffolds displayed a cell-killing effect on SAOS-eGFP cells compared to CD-HA 2%Sr.

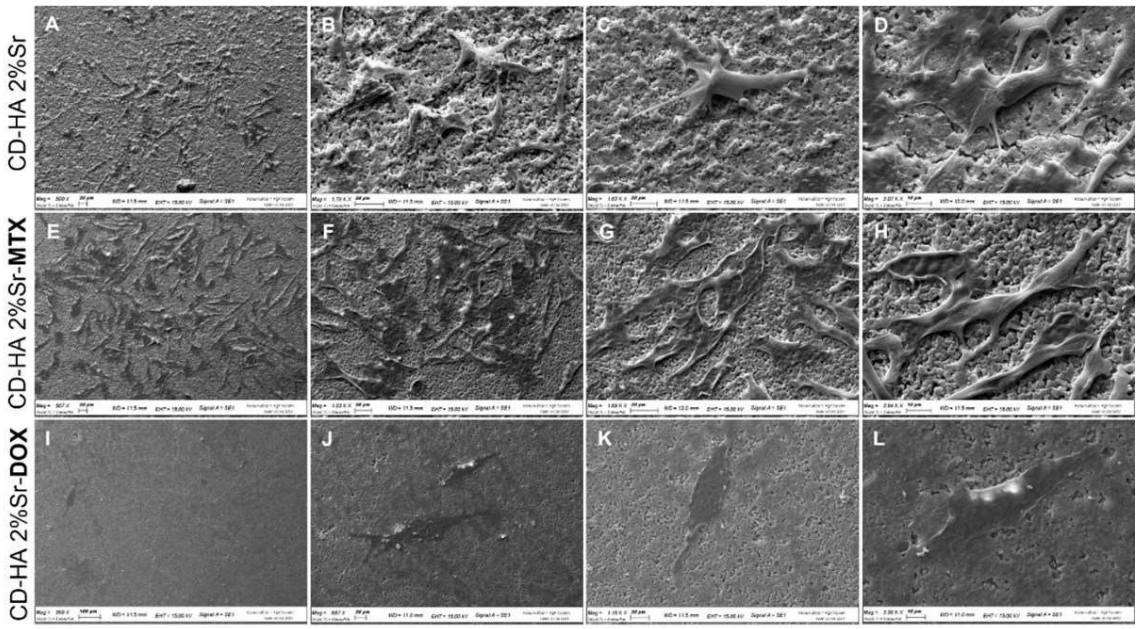

Figure 15. Scanning electron microscopy analysis of drug-linked CD-HA 2%Sr scaffolds and control with SAOS-eGFP cells. CD-HA 2%Sr scaffold was completely covered by SAOS-eGFP cells exhibiting normal morphology and cytoplasmatic extensions; Scale bar: 20 µm, 500X (A), Scale bar: 20 µm, 1.79K X (B), Scale bar: 20 µm, 1.62K X (C), Scale bar: 10 µm, 3.07K X (D), respectively. CD-HA 2%Sr-MTX scaffold was almost completely covered by SAOS-eGFP cells exhibiting a damaged morphology; Scale bar: 20 µm, 507X (E), Scale bar: 20 µm, 1.03K X (F), Scale bar: 20 µm, 1.69K X (G), Scale bar: 10 µm, 2.99K X (H), respectively. Few SAOS-eGFP cells were visible on CD-HA 2%Sr-DOX scaffold; Scale bar: 100 µm, 268X (I), Scale bar: 20 µm, 687 X (J), Scale bar: 20 µm, 1.15K X (K), Scale bar: 10 µm, 2.26K X (L), respectively.

4.5. Cytotoxic effects of CD-HA 2%Sr-MTX and CD-HA 2%Sr-DOX on SAOS-eGFP cells viability

The effects of CD-HA 2%Sr-MTX and CD-HA 2%Sr-DOX scaffolds on SAOS-eGFP cells viability were investigated by evaluating fluorescence intensity emitted from the engineered cell line at day 7.

Digital images obtained using a confocal microscope (LSM510; Carl Zeiss, Jena, Germany) revealed that the CD-HA 2%Sr scaffold was completely covered by SAOS-eGFP cells (Figure 16; Panel A); the number of SAOS-eGFP cells decreased in CD-HA

2%Sr-MTX (Figure 16; Panel B) and were mostly absent in CD-HA 2%Sr-DOX (Figure 16; Panel C). Quantification of fluorescence intensity confirmed the data from the confocal microscope. The fluorescence intensity means of SAOS-eGFP cells grown on the CD-HA 2%Sr scaffold was higher than for cells grown on CD-HA 2%Sr-MTX ($p<0.05$) and CD-HA 2%Sr-DOX ($p<0.005$). There were no statistical differences between the CD-HA 2%Sr-MTX and CD-HA 2%Sr-DOX groups (Figure 16; Panel D).

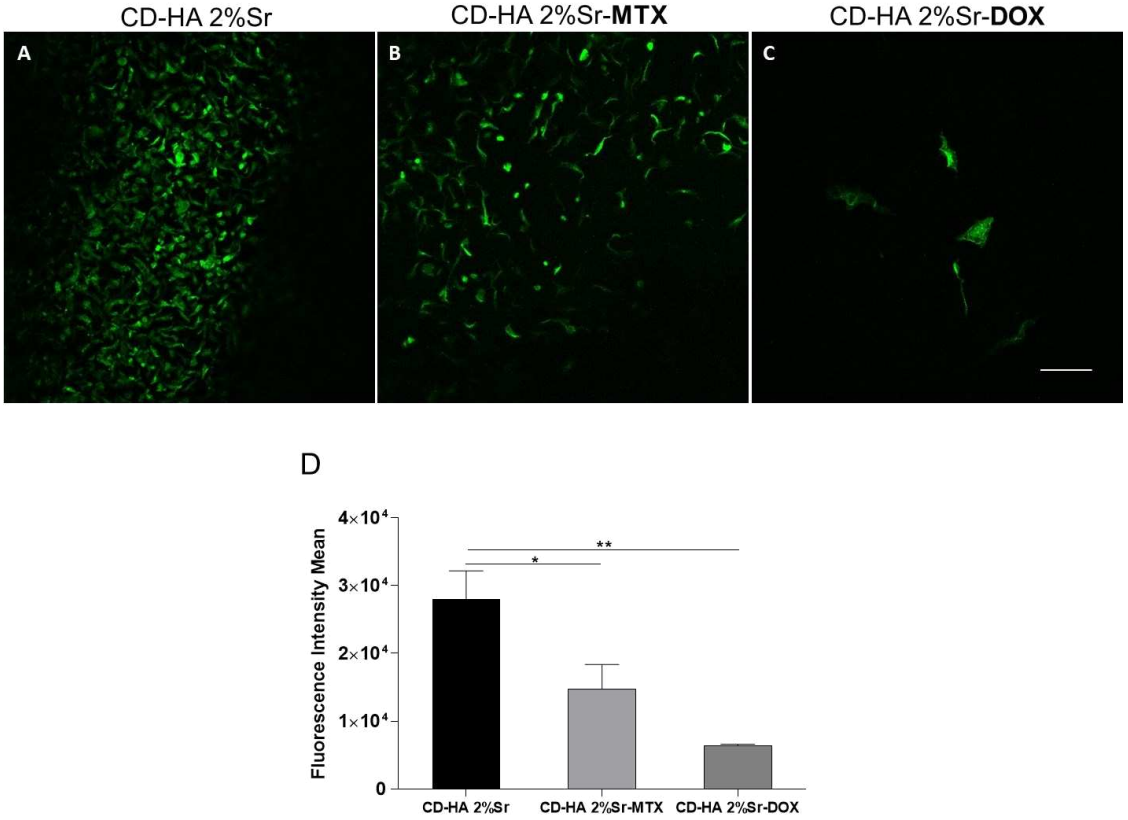

Figure 16. Fluorescence intensity evaluation of SAOS-eGFP cells grown on CD-HA 2%Sr-MTX and CD-HA 2%Sr-DOX scaffolds. Images acquired with confocal microscope of SAOS-eGFP cells on CD-HA 2%Sr (A), CD-HA 2%Sr-MTX (B), CD-HA 2%Sr-DOX (C). Z-stack images were collected at 0.5 µm slices by confocal microscopy from the bottom to the top of the cells and were merged into a single frame. Scale bar: 100 µm. Quantification of SAOS-eGFP cells fluorescence intensity with ImageJ software (D). CD-HA 2%Sr vs CD-HA 2%Sr-MTX, $p<0.05$; CD-HA 2%Sr vs CD-HA 2%Sr-DOX $p<0.005$.

4.6. Cytotoxic effects of CD-HA 2%Sr-MTX and CD-HA 2%Sr-DOX on SAOS-eGFP cells metabolic activity

The effects of CD-HA 2%Sr-MTX and CD-HA 2%Sr-DOX scaffolds on the metabolic activity of SAOS-eGFP cells were investigated using an Alamar Blue assay at days 1, 2 and 7. Results showed an increasing number of SAOS-eGFP cells grown on the control scaffold CD-HA 2%Sr; contrariwise, SAOS-eGFP cells increased in CD-HA 2%Sr-MTX and CD-HA 2%Sr-DOX during the first two days of culturing ($p>0.05$; Figure 17). However, at day 7 the number of SAOS-eGFP cells significantly decreased in MTX/DOX-conjugated scaffolds compared to CD-HA 2%Sr ($p<0.005$ and $p<0.001$; Figure 17). The number of SAOS-eGFP cells decreased in CD-HA 2%Sr-DOX compared to CD-HA 2%Sr-MTX ($p<0.005$; Figure 17).

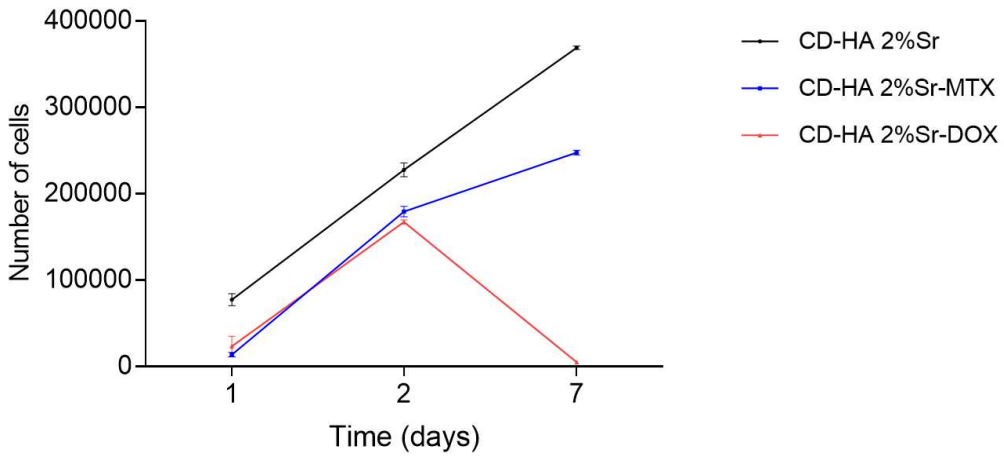

Figure 17. SAOS metabolic activity measured by AlamarBlue assay at days 1, 2, 7 of cell culture. Graph shows increasing number of SAOS-eGFP cells grown on CD-HA 2%Sr up to day 7. SAOS-eGFP cells increased on CD-HA 2%Sr-MTX, and CD-HA 2%Sr-DOX up to day 2 ($p>0.05$); whereas decreased on CD-HA 2%Sr-MTX, and CD-HA 2%Sr-DOX up to day 7 ($p<0.05$).

5. DISCUSSION

In the present study, an innovative scaffold made up of strontium-substituted nanostructured calcium-deficient hydroxyapatite (CD-HA 2%Sr) was investigated for its cytocompatibility and osteoinductivity using hASCs. The functionalized CD-HA 2%Sr scaffolds for drug-delivery of Methotrexate (CD-HA 2%Sr-MTX) and Doxorubicin (CD-HA 2%Sr-DOX) drugs were analysed for anti-cancer activity on SAOS-eGFP cells cultures. Viability analyses for metabolic activity and cell morphology conducted in hASCs has suggested that a CD-HA 2%Sr scaffold has the requirements for *in vitro* cytocompatibility. Indeed, an increasing number of live cells was observed on the tested scaffold as well as on the control using Alamar Blue and Live/Dead assays during the experimental time course. In addition, hASCs grown in contact with the CD-HA 2%Sr scaffold exhibit well-organised cytoskeleton architecture with actin filaments being distributed uniformly in cell cytoplasm at day 14. In addition, CD-HA 2%Sr biomaterial presents a highly-granular structure offering a good microenvironment for the adhesion and proliferation of hASCs as shown by SEM analysis where cells were well-established/attached on the scaffold surface.

Cellular biology results were supported by molecular biology data, such as gene expression analysis carried out using a PCR array technique to evaluate the extracellular matrix and cell adhesion molecules profile. In bone, ECM regulate cell adhesion, proliferation, and differentiation by synthetizing collagen, integrins, fibronectin and connective tissue growth factor [86]. Moreover, osteogenic differentiation during the ECM secretion phase in MSCs induces morphological changes in immature osteoblasts and it is immediately followed by the formation of mature osteoblasts [87]. Due to the

interconnection between ECM deposition and osteogenic differentiation in MSCs, some genes are shared and/or connected between commercial PCR Array plates for human ECM and Osteogenesis, therefore these aspects will be discussed together, below. In hASCs, genes encoding cell adhesion molecules were up-regulated in the presence of CD-HA 2%Sr scaffold, thus demonstrating the ability of the scaffold to mediate cell-cell and/or cell-scaffold interaction. Among them, *ICAM1*, *PECAM1*, *VCAM1*, *SELL* and *CD44* molecule up-regulation was observed. *SELL* is a calcium-dependent lectin that mediates cell adhesion by binding to glycoproteins on neighbouring cells [88], whereas the *CD44* molecule is responsible for cell-cell interactions engaging extracellular matrix components, such as hyaluronan/HA, collagen, growth factors, cytokines or proteases [89].

Cell interaction with ECM and adjacent cells is crucial for tissue morphogenesis and architecture, thus such actions are mediated by integrin and cadherins [90].

The CD-HA 2%Sr scaffold stimulated the up-regulation of genes encoding integrins and cadherins in hASCs. Early expressed integrins are *ITGA2* and *ITGB3* followed by *ITGA3*, *ITGA4*, *ITGA6* and *ITGA8* which were up-regulated at day 14. The gene expression levels of *ITGA2* and *ITGA3* were in agreement in the two different PCR-Arrays for ECM and Osteogenesis, as well as *ITGA1*, which resulted as down-regulated in both assays at the first time point. Of all the cadherins, *CDH1*, a calcium-dependent cell adhesion protein, resulted up-regulated in hASCs grown on the biomaterial. Integrins and cadherins have an important role in proper development, function, regeneration of skeletal tissue and MSCs osteogenic differentiation [90,91].

Collagen is the most abundant constituent of ECM acting as a mechanical support for cells [92]. *In vitro* results demonstrate that the CD-HA 2%Sr scaffold promoted the expression of genes encoding for collagen proteins including *COL7A1*, *COL8A1*, *COL11A1*, *COL14A1* and *COL15A1*. The latter is constantly up-expressed during the

experimental time course in the both the assay PCRs highlighting its important role in osteogenic differentiation and mineralization [93].

Another element, which is abundant in ECM is the hyaluronan matrix synthesized by hyaluronan synthase enzymes (HAS). *HAS1* gene expression was prompted by the CD-HA 2%Sr scaffold tested herein [94].

ECM undergoes remodelling thanks to the activity of ADAMTS proteins which have metallopeptidases functions [95,96]. *ADAMTS1*, *ADAMTS8*, and *ADAMTS13* expression was stimulated in hASCs by the CD-HA 2%Sr scaffold at day 14.

Matrix metalloproteinases (MMP), which have the ability to cleave collagens and proteoglycans, are among the most active proteases in ECM regulation [87]. These proteinases are involved in wound healing and tissue remodelling [97]. *MMP1*, *MMP3* and *MMP11* gene expression was promptly induced by CD-HA 2%Sr in hASCs. *MMP15* and *MMP8* were positively modulated by the scaffold later. Indeed, while *MMP15* is a membrane-type metalloproteinase [98], *MMP8* is expressed in osteoblastic progenitors, differentiated osteoblasts, and osteocytes [99]. Moreover, *MMP10* resulted positively modulated by CD-HA 2%Sr in hASCs. *MMP10* is essential for human bone development [100] and takes part in the physiological processes of bone growth [101].

The *BMP2* gene resulted up-regulated in our experiments suggesting hASCs osteogenic differentiation upon contact with the scaffold. Further, it has been reported that *MMP10* enhances *BMP-2*-induced osteoblast differentiation *in vitro* [102].

The crucial signalling pathways leading MSCs towards osteogenesis differentiation are transforming growth factor-beta (TGF-β) and bone morphogenic protein (BMP) [61,103]. Our results demonstrate that CD-HA 2%Sr scaffold up-regulated genes are involved in these two signalling cascades, highlighting its osteoinductivity property. Specifically, three of the most important BMPs involved in osteogenesis, i.e., *BMP2*, *BMP4*, and *BMP7* resulted up-regulated alongside other BMP signalling factors like *BMPR1A*,

BMPR2 and *SMAD5* [104]. On the other hand, of all the factors involved in the TGF-β cascade, *TGFBR1*, *TGFBR2* were positively regulated from scaffold.

The activation of the cited signalling pathways leads to the expression of master osteogenic transcription factors, such as *RUNX2* and *Osterix* (*OSX*), also known as *SP7*. More precisely, *OSX* is a downstream *RUNX2* gene [105]. Our results are in agreement with published reports in as much as they demonstrated that the *RUNX2* gene was up-regulated at day 3 and 6, whereas *SP7* expression with high fold change is observed at day 14 when *RUNX2* modulation disappears. Finally, *RUNX2* and *SP7* activity results in specific osteoblast gene expression of including osteocalcin and collagen [105]. CD-HA 2%Sr biomaterial induced osteocalcin up-regulation in term of gene (*BGLAP*) and protein expression (OCN). These results were corroborated with analysis of matrix mineralization showing an increase matrix deposition in hASCs grown on the scaffold compared to the revealing *ALPL* gene up-regulation. Altogether this evidence validated the osteoinductivity capacity of the CD-HA 2%Sr scaffold.

Other osteogenic genes involved in the skeletal development process were modulated in hASCs by the scaffold. Of these, up-regulation of *GLI1* and *EGFR* was observed. *GLI1* is a transcriptional activator involved in signalling-mediated specification for osteoblast lineage inducing early osteoblast differentiation [106]. On the other hand, *EGFR* takes part in EGFR/ERK/IGFBP-3 signalling pathway inducing osteoblast differentiation and maturation [55].

Additionally, the *CLEC3B* gene was found to be expressed in hASCs grown on the biomaterial at up to day 14. The encoded protein binds Ca^{2+} and it is involved in bone metabolism, indeed it was detected in response to osteoinduction [107].

It is well known that when MSCs differentiate into osteoblasts many osteoclast-associated cytokines are secreted, including *CSF*, *RANKL* stimulating osteoclast differentiation [108]. Our experiments revealed the up-regulation of *TNFSF11*, also known as *RANKL*,

and *CSF2/3* genes. This indicates that in differentiating hASCs the mechanism of bone resorption is activated alongside the bone formation process. The coupled mechanisms continuously lead to bone remodelling.

Although cell biology and gene expression results highlighted osteoinductivity properties in the CD-HA 2% scaffold, *SPP1* was found to be down-regulated. *SPP1* gene encodes osteopontin (OPN), a protein expressed in bone ECM [109]. Consideration of SPP1 as a late marker of osteogenesis may explain its down-regulation in our results [110]. Additionally, investigations into the OPN protein expression revealed no modulation of this protein in hASCs in contact with the scaffold (data not shown). Further characterization is needed to clarify *SPP1* down-modulation.

Overall, the expression of the most important genes involved in ECM deposition and skeletal development, alongside cellular biology results, validated the cytocompatibility and ostoinductivity features of CD-HA 2% scaffold in hASCs.

OS is the most common bone malignancy to be primarily diagnosed in children and adolescents [111]. OS treatment generally consists of surgery in association with chemotherapy. The adverse effects, and in some case the ineffectiveness, of this treatment plan has stimulated scientists and surgeons to identify new therapeutic strategies. Innovative scaffolds designed as drug-delivery systems with bone regenerative properties may represent a valid therapeutic alternative to OS care. The ability of functionalized CD-HA 2%Sr scaffolds to contrast OS cells proliferation was assessed *in vitro* using the SAOS-eGFP cell line which represents the most appropriate study model as previously reported [40,47,112,113]. The CD-HA 2%Sr biomaterials were linked to the most frequently used anti-cancer drugs for treating OS, such as Methotrexate (CD-HA 2%Sr-MTX) and Doxorubicin (CD-HA 2%Sr-DOX) [16,18,19].

The CD-HA 2%Sr-MTX and CD-HA 2%Sr-DOX drug-linked scaffolds were prepared to release approximately 45µg/mL and 5µg/mL of the drug, respectively. Since there are

no previous studies investigating CD-HA 2%Sr scaffolds as a drug delivery system, the DOX concentration was chosen according to the data obtained in different scaffold with similar composition [47]. Contrariwise, in the literature there are heterogeneous data about the MTX concentration used, which range from 0.1 – 100 μM [114], and >100μM in case of primary SAOS cell line [114].

CD-HA 2%Sr-MTX and CD-HA 2%Sr-DOX scaffolds exert an *in vitro* anti-proliferative capacity on SAOS-eGFP cells as suggested by these experimental results. Indeed, a decreasing number of SAOS-eGFP cells were observed at day 7 in MTX/DOX-conjugated scaffolds compared to CD-HA 2%Sr. These data were supported by qualitative and quantitative results obtained by analysing fluorescence from engineered SAOS. Indeed, images from a confocal microscope and measurement of fluorescence intensity revealed reduced numbers of SAOS on CD-HA 2%Sr-MTX compared to the control and very few SAOS-eGFP cells in the CD-HA 2%Sr-DOX scaffold. Similarly, SEM investigation allowed to analyse cell morphology of cell on the scaffolds. Microscopic observation allowed to appreciate how the CD-HA 2%Sr scaffold surface was completely covered with SAOS-eGFP cells with their natural morphology. Contrariwise, when SAOS-eGFP cells was in contact with CD-HA 2%Sr-MTX they presented altered morphology, although these were found over the entire surface. Only a few SAOS-eGFP cells were observed on the CD-HA 2%Sr-DOX scaffold. Overall, these results are in agreement with the different experiments which were performed suggesting the cytotoxic effects of MTX and DOX drug concentrations. Nevertheless, it is evident that 5μg/mL of DOX displayed a cell-killing effect on SAOS-eGFP cells higher than 45μg/mL of MTX was used. MTX concentration is probably not enough to destroy a SAOS cell line as reported from Suksiriworapong et al., [112]. Contrariwise, DOX concentration could be reduced, as indicated by Zhou et al., [113].

Overall, SAOS-eGFP cells reduction in terms of cell numbers and fluorescence intensity, as well as the damaged morphology of cells grown on MTX/DOX- conjugated CD-HA 2%Sr scaffolds compared to the control, validated the anti-proliferative properties in these scaffolds on OS cells. Nevertheless, further investigations are needed to better characterize the antineoplastic activity of these innovative materials.

6. CONCLUSIONS

CD-HA 2%Sr scaffold has been analysed for its cytocompatibility and osteoinductivity characteristics. *In vitro* experiments also revealed that CD-HA 2%Sr is cytocompatible and osteoinductive, as attested by the overexpression of various genes involved in ECM deposition and osteogenic processes including integrins (*ITGA2*, *ITGA3*, *ITGA4*, *ITGA6*, *ITGA8*, and *ITGB3*), cadherins (*CDH1*), collagens (*COL7A1*, *COL8A1*, *COL11A1*, *COL14A1*, *COL15A1*) and MMPs (*MMP1*, *MMP3*, *MMP8*, *MMP10*, *MMP11* and *MMP15*), as well as genes involved in TGF-β and BMP signalling pathways (*TGFBR1*, *TGFBR2*, *BMP2*, *BMP4*, *BMP7*, *SMAD5*), skeletal development (*RUNX2*, *SP7*, *ALPL*, *OCN*) and osteoclastic differentiation (*CSF2*, *CSF3* and *RANKL*) which were detected in hASCs grown on scaffolds at up to 14 days.

OS is an aggressive malignant neoplasm, which mainly affects paediatric and young adult patients. Ineffective and controversial OS treatment, as well as its adverse effects, has prompted researchers to seek novel therapeutic options, which are able to go beyond these limitations and improve patient survival. In this study, innovative scaffolds made of strontium substituted nanostructured calcium-deficient hydroxyapatite (CD-HA 2%Sr) functionalized as a drug-delivery system for Methotrexate (CD-HA 2%Sr-MTX) and Doxorubicin (CD-HA 2%Sr-DOX) have been tested *in vitro* as a novel therapeutic strategy to contrast OS cell proliferation.

Preliminary *in vitro* experiments carried out on the drug-linked scaffolds have revealed the cytotoxic effects of the released drugs in SAOS-eGFP cells after 7 days. The 5µg/mL of DOX released by the CD-HA 2%Sr scaffold resulted more effective than 45µg/mL of

MTX. Further *in vitro* investigations are thus needed to verify the genetic and epigenetic influences of these drug-delivery scaffolds.

7. FUTURE PERSPECTIVES

Although the cytocompatibility and osteoinductivity of CD-HA 2%Sr scaffold have been extensively analysed, the antineoplastic activity of CD-HA 2%Sr-MTX and CD-HA 2%Sr-DOX remains to be further investigated. Analysis of different drug concentrations, are necessary in order to identify the right dose of MTX and DOX released from these innovative scaffolds. Specifically, our results suggest the use of a > 45µg/mL concentration for MTX and < 5µg/mL for DOX. Further investigations will be carried out by analysing cancer cells viability grown on scaffolds that release a drug concentration ten times lower and higher than the already tested concentrations of MTX and DOX, respectively. Cell viability will be performed with Alamar Blue assay as previous experiments.

HASCs present an ideal stem cell source for practical regenerative medicine, thanks to their abundant availability, immunomodulation, homing activity, paracrine effects, and differentiation ability [115]. Indeed, in the present study, this kind of cells played a central role to investigate the cytocompatibility and osteoinductivity proprieties of the CD-HA 2%Sr scaffolds. Since their ability to enhance tissues regeneration in combination with biomaterials, hASCs will be further investigated to know their behaviour in contact with drugs. Therefore, the effects of drug-released scaffolds on hASCs and non-tumoral osteoblasts should be analysed. To this purpose, 2D and 3D cell co-cultures of hASCs and cancer cells (SAOS-2) will be set up in order to evaluate the anti-proliferative capacity of MTX and DOX on SAOS-2 as well as the absence of cytotoxic effects on hASCs. Similarly, co-cultures of normal human osteoblasts (HObs) and SAOS-2 cells will be performed to well-characterize the effect of the scaffolds on bone

microenvironment. Cell viability will be investigated through Alamar blue assay with the same conditions as the former experiments. In addition, analyses for hASCs, HObs and SAOS-2 viability grown on the MTX/DOX-linked scaffolds will be confirmed with MTT (3-(4,5-dimethylthiazol-2-yl)-2,5-diphenyltetrazolium bromide) assay which is the most widely exploited approach in cancer research to analyse cell proliferation, viability and drug cytotoxicity [116]. In the aforementioned cellular models, analyses of human apoptosis genes and proteins modulated by CD-HA 2%Sr-MTX and CD-HA 2%Sr-DOX will be carried out. In particular, cell death and the involvement of apoptosis will be assessed using 2D and 3D co-culture models by analysing of Caspase 3 expression protein, AnnexinV/PI, Hoechst 33342, and Live/Dead staining.

Finally, the effectiveness of CD-HA 2%Sr-MTX and CD-HA 2%Sr-DOX as a treatment for killing cancer cells will be evaluated *in vivo* in a mouse OS model. After approval by ethics committee, *in vivo* study foresee the establishment of xenograft tumours in male nude mice through SAOS-2 cells subcutaneously inoculation. Nude mice models will be divided in three different experimental groups in which CD-HA 2%Sr-MTX (i), CD-HA 2%Sr-DOX (ii) and CD-HA 2%Sr (iii) scaffolds, as control, should be implanted. Osteosarcoma progression and adverse effects of the scaffolds should be monitored with X-ray analysis. Promising results of pre-clinical studies could allow the clinical translation of drug-linked CD-HA 2%Sr scaffolds.

REFERENCES

1. Habibovic, P. * Strategic Directions in Osteoinduction and Biomimetics. *Tissue Eng. Part A* **2017**, *23*, 1295–1296, doi:10.1089/ten.TEA.2017.0430.
2. Arvidson, K.; Abdallah, B.M.; Applegate, L.A.; Baldini, N.; Cenni, E.; Gomez-Barrena, E.; Granchi, D.; Kassem, M.; Konttinen, Y.T.; Mustafa, K.; et al. Bone Regeneration and Stem Cells. *J. Cell. Mol. Med.* **2011**, *15*, 718–746, doi:10.1111/j.1582-4934.2010.01224.x.
3. Wade, S.W.; Strader, C.; Fitzpatrick, L.A.; Anthony, M.S.; O'Malley, C.D. Estimating Prevalence of Osteoporosis: Examples from Industrialized Countries. *Arch. Osteoporos.* **2014**, *9*, 182, doi:10.1007/s11657-014-0182-3.
4. Iaquinta, M.R.; Mazzoni, E.; Manfrini, M.; D'Agostino, A.; Trevisiol, L.; Nocini, R.; Trombelli, L.; Barbanti-Brodano, G.; Martini, F.; Tognon, M. Innovative Biomaterials for Bone Regrowth. *Int. J. Mol. Sci.* **2019**, *20*, doi:10.3390/ijms20030618.
5. Binkley, N.; Buehring, B. Beyond FRAX: It's Time to Consider "Sarco-Osteopenia." *J. Clin. Densitom. Off. J. Int. Soc. Clin. Densitom.* **2009**, *12*, 413–416, doi:10.1016/j.jocd.2009.06.004.
6. Jackson, T.M.; Bittman, M.; Granowetter, L. Pediatric Malignant Bone Tumors: A Review and Update on Current Challenges, and Emerging Drug Targets. *Curr. Probl. Pediatr. Adolesc. Health Care* **2016**, *46*, 213–228, doi:10.1016/j.cppeds.2016.04.002.
7. Chindamo, G.; Sapino, S.; Peira, E.; Chirio, D.; Gonzalez, M.C.; Gallarate, M. Bone Diseases: Current Approach and Future Perspectives in Drug Delivery Systems for Bone Targeted Therapeutics. *Nanomater. Basel Switz.* **2020**, *10*, E875, doi:10.3390/nano10050875.
8. Mirabello, L.; Troisi, R.J.; Savage, S.A. International Osteosarcoma Incidence Patterns in Children and Adolescents, Middle Ages and Elderly Persons. *Int. J. Cancer* **2009**, *125*, 229–234, doi:10.1002/ijc.24320.
9. Ritter, J.; Bielack, S.S. Osteosarcoma. *Ann. Oncol. Off. J. Eur. Soc. Med. Oncol.* **2010**, *21 Suppl 7*, vii320-325, doi:10.1093/annonc/mdq276.

10. Kumar, R.; Kumar, M.; Malhotra, K.; Patel, S. Primary Osteosarcoma in the Elderly Revisited: Current Concepts in Diagnosis and Treatment. *Curr. Oncol. Rep.* **2018**, *20*, 13, doi:10.1007/s11912-018-0658-1.
11. Ottaviani, G.; Jaffe, N. The Epidemiology of Osteosarcoma. *Cancer Treat. Res.* **2009**, *152*, 3–13, doi:10.1007/978-1-4419-0284-9_1.
12. Jafari, F.; Javdansirat, S.; Sanaie, S.; Naseri, A.; Shamekh, A.; Rostamzadeh, D.; Dolati, S. Osteosarcoma: A Comprehensive Review of Management and Treatment Strategies. *Ann. Diagn. Pathol.* **2020**, *49*, 151654, doi:10.1016/j.anndiagpath.2020.151654.
13. Egea-Gámez, R.M.; Ponz-Lueza, V.; Cendrero-Torrado, A.; Martínez-González, C.; Certucha-Barragán, J.A.; González-Díaz, R. Spinal Osteosarcoma in the Paediatric Age Group: Case Series and Literature Review. *Rev. Espanola Cirugia Ortop. Traumatol.* **2019**, *63*, 122–131, doi:10.1016/j.recot.2018.09.001.
14. Prater, S.; McKeon, B. Osteosarcoma. In *StatPearls*; StatPearls Publishing: Treasure Island (FL), 2021.
15. Misaghi, A.; Goldin, A.; Awad, M.; Kulidjian, A.A. Osteosarcoma: A Comprehensive Review. *SICOT-J* **2018**, *4*, 12, doi:10.1051/sicotj/2017028.
16. Beaury, M.W.; Kelly-Beaury, M.L.; Sharp, G.; Cottrell, J.A. A Review of Osteosarcoma Therapeutics. *J. Cancer Treat. Diagn.* **2018**, *2*.
17. Lewis, V.O. Limb Salvage in the Skeletally Immature Patient. *Curr. Oncol. Rep.* **2005**, *7*, 285–292, doi:10.1007/s11912-005-0052-7.
18. Yu, D.; Zhang, S.; Feng, A.; Xu, D.; Zhu, Q.; Mao, Y.; Zhao, Y.; Lv, Y.; Han, C.; Liu, R.; et al. Methotrexate, Doxorubicin, and Cisplatinum Regimen Is Still the Preferred Option for Osteosarcoma Chemotherapy: A Meta-Analysis and Clinical Observation. *Medicine (Baltimore)* **2019**, *98*, e15582, doi:10.1097/MD.0000000000015582.
19. Xu, M.; Xu, S.F.; Yu, X.C. Clinical Analysis of Osteosarcoma Patients Treated with High-Dose Methotrexate-Free Neoadjuvant Chemotherapy. *Curr. Oncol. Tor. Ont* **2014**, *21*, e678-684, doi:10.3747/co.21.1973.
20. Bacci, G.; Briccoli, A.; Rocca, M.; Ferrari, S.; Donati, D.; Longhi, A.; Bertoni, F.; Bacchini, P.; Giacomini, S.; Forni, C.; et al. Neoadjuvant Chemotherapy for Osteosarcoma of the Extremities with Metastases at Presentation: Recent Experience at the Rizzoli Institute in 57 Patients Treated with Cisplatin,

Doxorubicin, and a High Dose of Methotrexate and Ifosfamide. *Ann. Oncol. Off. J. Eur. Soc. Med. Oncol.* **2003**, *14*, 1126–1134, doi:10.1093/annonc/mdg286.

21. Harrison, D.J.; Schwartz, C.L. Osteogenic Sarcoma: Systemic Chemotherapy Options for Localized Disease. *Curr. Treat. Options Oncol.* **2017**, *18*, 24, doi:10.1007/s11864-017-0464-2.
22. Janeway, K.A.; Grier, H.E. Sequelae of Osteosarcoma Medical Therapy: A Review of Rare Acute Toxicities and Late Effects. *Lancet Oncol.* **2010**, *11*, 670–678, doi:10.1016/S1470-2045(10)70062-0.
23. Ho-Shui-Ling, A.; Bolander, J.; Rustom, L.E.; Johnson, A.W.; Luyten, F.P.; Picart, C. Bone Regeneration Strategies: Engineered Scaffolds, Bioactive Molecules and Stem Cells Current Stage and Future Perspectives. *Biomaterials* **2018**, *180*, 143–162, doi:10.1016/j.biomaterials.2018.07.017.
24. Murugan, R.; Ramakrishna, S. Development of Nanocomposites for Bone Grafting. *Compos. Sci. Technol.* **2005**, *65*, 2385–2406, doi:10.1016/j.compscitech.2005.07.022.
25. Kaur, G.; Pandey, O.P.; Singh, K.; Homa, D.; Scott, B.; Pickrell, G. A Review of Bioactive Glasses: Their Structure, Properties, Fabrication and Apatite Formation. *J. Biomed. Mater. Res. A* **2014**, *102*, 254–274, doi:10.1002/jbm.a.34690.
26. Montesi, M.; Panseri, S.; Dapporto, M.; Tampieri, A.; Sprio, S. Sr-Substituted Bone Cements Direct Mesenchymal Stem Cells, Osteoblasts and Osteoclasts Fate. *PloS One* **2017**, *12*, e0172100, doi:10.1371/journal.pone.0172100.
27. Costa-Pinto, A.R.; Reis, R.L.; Neves, N.M. Scaffolds Based Bone Tissue Engineering: The Role of Chitosan. *Tissue Eng. Part B Rev.* **2011**, *17*, 331–347, doi:10.1089/ten.teb.2010.0704.
28. Wang, L.; Stegemann, J.P. Thermogelling Chitosan and Collagen Composite Hydrogels Initiated with Beta-Glycerophosphate for Bone Tissue Engineering. *Biomaterials* **2010**, *31*, 3976–3985, doi:10.1016/j.biomaterials.2010.01.131.
29. Costa-Pinto, A.R.; Correlo, V.M.; Sol, P.C.; Bhattacharya, M.; Srouji, S.; Livne, E.; Reis, R.L.; Neves, N.M. Chitosan-Poly(Butylene Succinate) Scaffolds and Human Bone Marrow Stromal Cells Induce Bone Repair in a Mouse Calvaria Model. *J. Tissue Eng. Regen. Med.* **2012**, *6*, 21–28, doi:10.1002/term.391.

30. Gentile, P.; Chiono, V.; Carmagnola, I.; Hatton, P.V. An Overview of Poly(Lactic-Co-Glycolic) Acid (PLGA)-Based Biomaterials for Bone Tissue Engineering. *Int. J. Mol. Sci.* **2014**, *15*, 3640–3659, doi:10.3390/ijms15033640.
31. Remya, K.R.; Joseph, J.; Mani, S.; John, A.; Varma, H.K.; Ramesh, P. Nanohydroxyapatite Incorporated Electrospun Polycaprolactone/Polycaprolactone-Polyethyleneglycol-Polycaprolactone Blend Scaffold for Bone Tissue Engineering Applications. *J. Biomed. Nanotechnol.* **2013**, *9*, 1483–1494, doi:10.1166/jbn.2013.1640.
32. Arafat, M.T.; Lam, C.X.F.; Ekaputra, A.K.; Wong, S.Y.; Li, X.; Gibson, I. Biomimetic Composite Coating on Rapid Prototyped Scaffolds for Bone Tissue Engineering. *Acta Biomater.* **2011**, *7*, 809–820, doi:10.1016/j.actbio.2010.09.010.
33. Mazzoni, E.; D'Agostino, A.; Manfrini, M.; Maniero, S.; Puozzo, A.; Bassi, E.; Marsico, S.; Fortini, C.; Trevisiol, L.; Patergnani, S.; et al. Human Adipose Stem Cells Induced to Osteogenic Differentiation by an Innovative Collagen/Hydroxylapatite Hybrid Scaffold. *FASEB J. Off. Publ. Fed. Am. Soc. Exp. Biol.* **2017**, *31*, 4555–4565, doi:10.1096/fj.201601384R.
34. Wang, J.-L.; Chen, Q.; Du, B.-B.; Cao, L.; Lin, H.; Fan, Z.-Y.; Dong, J. Enhanced Bone Regeneration Composite Scaffolds of PLLA/β-TCP Matrix Grafted with Gelatin and HAp. *Mater. Sci. Eng. C Mater. Biol. Appl.* **2018**, *87*, 60–69, doi:10.1016/j.msec.2018.02.011.
35. Ghosh, S.; Ghosh, S.; Jana, S.K.; Pramanik, N. Biomedical Application of Doxorubicin Coated Hydroxyapatite-Poly(Lactide-Co-Glycolide) Nanocomposite for Controlling Osteosarcoma Therapeutics. *J. Nanosci. Nanotechnol.* **2020**, *20*, 3994–4004, doi:10.1166/jnn.2020.17689.
36. Bischoff, I.; Tsaryk, R.; Chai, F.; Fürst, R.; Kirkpatrick, C.J.; Unger, R.E. In Vitro Evaluation of a Biomaterial-Based Anticancer Drug Delivery System as an Alternative to Conventional Post-Surgery Bone Cancer Treatment. *Mater. Sci. Eng. C Mater. Biol. Appl.* **2018**, *93*, 115–124, doi:10.1016/j.msec.2018.07.057.
37. Bae, Y.H.; Park, K. Targeted Drug Delivery to Tumors: Myths, Reality and Possibility. *J. Control. Release Off. J. Control. Release Soc.* **2011**, *153*, 198–205, doi:10.1016/j.jconrel.2011.06.001.
38. Wilhelm, S.; Tavares, A.J.; Dai, Q.; Ohta, S.; Audet, J.; Dvorak, H.F.; Chan, W.C.W. Analysis of Nanoparticle Delivery to Tumours. *Nat. Rev. Mater.* **2016**, *1*, 1–12, doi:10.1038/natrevmats.2016.14.

39. Liu, Y.; Raina, D.B.; Sebastian, S.; Nagesh, H.; Isaksson, H.; Engellau, J.; Lidgren, L.; Tägil, M. Sustained and Controlled Delivery of Doxorubicin from an In-Situ Setting Biphasic Hydroxyapatite Carrier for Local Treatment of a Highly Proliferative Human Osteosarcoma. *Acta Biomater.* **2021**, *131*, 555–571, doi:10.1016/j.actbio.2021.07.016.
40. Sarda, S.; Iafisco, M.; Pascaud-Mathieu, P.; Adamiano, A.; Montesi, M.; Panseri, S.; Marsan, O.; Thouron, C.; Dupret-Bories, A.; Tampieri, A.; et al. Interaction of Folic Acid with Nanocrystalline Apatites and Extension to Methotrexate (Antifolate) in View of Anticancer Applications. *Langmuir ACS J. Surf. Colloids* **2018**, *34*, 12036–12048, doi:10.1021/acs.langmuir.8b02602.
41. Marques, C.; Ferreira, J.M.F.; Andronescu, E.; Ficai, D.; Sonmez, M.; Ficai, A. Multifunctional Materials for Bone Cancer Treatment. *Int. J. Nanomedicine* **2014**, *9*, 2713–2725, doi:10.2147/IJN.S55943.
42. Iafisco, M.; Margiotta, N. Silica Xerogels and Hydroxyapatite Nanocrystals for the Local Delivery of Platinum-Bisphosphonate Complexes in the Treatment of Bone Tumors: A Mini-Review. *J. Inorg. Biochem.* **2012**, *117*, 237–247, doi:10.1016/j.jinorgbio.2012.06.004.
43. Netz, D.J.; Sepulveda, P.; Pandolfelli, V.C.; Spadaro, A.C.; Alencastre, J.B.; Bentley, M.V.; Marchetti, J.M. Potential Use of Gelcasting Hydroxyapatite Porous Ceramic as an Implantable Drug Delivery System. *Int. J. Pharm.* **2001**, *213*, 117–125, doi:10.1016/s0378-5173(00)00659-1.
44. Palazzo, B.; Iafisco, M.; Laforgia, M.; Margiotta, N.; Natile, G.; Bianchi, C.L.; Walsh, D.; Mann, S.; Roveri, N. Biomimetic Hydroxyapatite–Drug Nanocrystals as Potential Bone Substitutes with Antitumor Drug Delivery Properties. *Adv. Funct. Mater.* **2007**, *17*, 2180–2188, doi:10.1002/adfm.200600361.
45. Andronescu, E.; Ficai, A.; Albu, M.G.; Mitran, V.; Sonmez, M.; Ficai, D.; Ion, R.; Cimpean, A. Collagen-Hydroxyapatite/Cisplatin Drug Delivery Systems for Locoregional Treatment of Bone Cancer. *Technol. Cancer Res. Treat.* **2013**, *12*, 275–284, doi:10.7785/tcrt.2012.500331.
46. Ficai, D.; Sonmez, M.; Albu, M.G.; Mihaiescu, D.E.; Ficai, A.; Bleotu, C. Antitumoral Materials with Regenerative Function Obtained Using a Layer-by-Layer Technique. *Drug Des. Devel. Ther.* **2015**, *9*, 1269–1279, doi:10.2147/DDDT.S62805.

47. Iafisco, M.; Drouet, C.; Adamiano, A.; Pascaud, P.; Montesi, M.; Panseri, S.; Sarda, S.; Tampieri, A. Superparamagnetic Iron-Doped Nanocrystalline Apatite as a Delivery System for Doxorubicin. *J. Mater. Chem. B* **2016**, *4*, 57–70, doi:10.1039/c5tb01524c.
48. Iaquinta, M.R.; Mazzoni, E.; Bononi, I.; Rotondo, J.C.; Mazziotta, C.; Montesi, M.; Sprio, S.; Tampieri, A.; Tognon, M.; Martini, F. Adult Stem Cells for Bone Regeneration and Repair. *Front. Cell Dev. Biol.* **2019**, *7*, 268, doi:10.3389/fcell.2019.00268.
49. Mazzoni, E.; Mazziotta, C.; Iaquinta, M.R.; Lanzillotti, C.; Fortini, F.; D'agostino, A.; Trevisiol, L.; Nocini, R.; Barbanti-Brodano, G.; Mescola, A.; et al. Enhanced Osteogenic Differentiation of Human Bone Marrow-Derived Mesenchymal Stem Cells by a Hybrid Hydroxylapatite/Collagen Scaffold. *Front. Cell Dev. Biol.* **2020**, *8*, doi:10.3389/fcell.2020.610570.
50. Batta, K.; Menegatti, S.; Garcia-Alegria, E.; Florkowska, M.; Lacaud, G.; Kouskoff, V. Concise Review: Recent Advances in the In Vitro Derivation of Blood Cell Populations. *Stem Cells Transl. Med.* **2016**, *5*, 1330–1337, doi:10.5966/sctm.2016-0039.
51. Globig, P.; Willumeit-Römer, R.; Martini, F.; Mazzoni, E.; Luthringer-Feyerabend, B.J.C. Optimizing an Osteosarcoma-Fibroblast Coculture Model to Study Antitumoral Activity of Magnesium-Based Biomaterials. *Int. J. Mol. Sci.* **2020**, *21*, doi:10.3390/ijms21145099.
52. Pearson, S.; Cuvertino, S.; Fleury, M.; Lacaud, G.; Kouskoff, V. In Vivo Repopulating Activity Emerges at the Onset of Hematopoietic Specification during Embryonic Stem Cell Differentiation. *Stem Cell Rep.* **2015**, *4*, 431–444, doi:10.1016/j.stemcr.2015.01.003.
53. Bianco, P.; Robey, P.G.; Simmons, P.J. Mesenchymal Stem Cells: Revisiting History, Concepts, and Assays. *Cell Stem Cell* **2008**, *2*, 313–319, doi:10.1016/j.stem.2008.03.002.
54. Mahmoudifar, N.; Doran, P.M. Mesenchymal Stem Cells Derived from Human Adipose Tissue. *Methods Mol. Biol. Clifton NJ* **2015**, *1340*, 53–64, doi:10.1007/978-1-4939-2938-2_4.
55. Mazzoni, E.; D'Agostino, A.; Iaquinta, M.R.; Bononi, I.; Trevisiol, L.; Rotondo, J.C.; Patergnani, S.; Giorgi, C.; Gunson, M.J.; Arnett, G.W.; et al. Hydroxylapatite-Collagen Hybrid Scaffold Induces Human Adipose-Derived

Mesenchymal Stem Cells to Osteogenic Differentiation in Vitro and Bone Regrowth in Patients. *Stem Cells Transl. Med.* **2020**, *9*, 377–388, doi:10.1002/sctm.19-0170.

56. Galderisi, U.; Giordano, A. The Gap between the Physiological and Therapeutic Roles of Mesenchymal Stem Cells. *Med. Res. Rev.* **2014**, *34*, 1100–1126, doi:10.1002/med.21322.
57. Ferro, F.; Spelat, R.; Baheney, C.S. Dental Pulp Stem Cell (DPSC) Isolation, Characterization, and Differentiation. *Methods Mol. Biol. Clifton NJ* **2014**, *1210*, 91–115, doi:10.1007/978-1-4939-1435-7_8.
58. Fei, X.; Jiang, S.; Zhang, S.; Li, Y.; Ge, J.; He, B.; Goldstein, S.; Ruiz, G. Isolation, Culture, and Identification of Amniotic Fluid-Derived Mesenchymal Stem Cells. *Cell Biochem. Biophys.* **2013**, *67*, 689–694, doi:10.1007/s12013-013-9558-z.
59. Fierabracci, A.; Lazzari, L.; Muraca, M.; Parolini, O. How Far Are We from the Clinical Use of Placental-Derived Mesenchymal Stem Cells? *Expert Opin. Biol. Ther.* **2015**, *15*, 613–617, doi:10.1517/14712598.2015.1000856.
60. Gong, X.; Sun, Z.; Cui, D.; Xu, X.; Zhu, H.; Wang, L.; Qian, W.; Han, X. Isolation and Characterization of Lung Resident Mesenchymal Stem Cells Capable of Differentiating into Alveolar Epithelial Type II Cells. *Cell Biol. Int.* **2014**, *38*, 405–411, doi:10.1002/cbin.10240.
61. Mazziotta, C.; Lanzillotti, C.; Iaquinta, M.R.; Taraballi, F.; Torreggiani, E.; Rotondo, J.C.; Otòn-Gonzalez, L.; Mazzoni, E.; Frontini, F.; Bononi, I.; et al. MicroRNAs Modulate Signaling Pathways in Osteogenic Differentiation of Mesenchymal Stem Cells. *Int. J. Mol. Sci.* **2021**, *22*, 2362, doi:10.3390/ijms22052362.
62. Loi, F.; Córdova, L.A.; Pajarinen, J.; Lin, T.; Yao, Z.; Goodman, S.B. Inflammation, Fracture and Bone Repair. *Bone* **2016**, *86*, 119–130, doi:10.1016/j.bone.2016.02.020.
63. Kitaori, T.; Ito, H.; Schwarz, E.M.; Tsutsumi, R.; Yoshitomi, H.; Oishi, S.; Nakano, M.; Fujii, N.; Nagasawa, T.; Nakamura, T. Stromal Cell-Derived Factor 1/CXCR4 Signaling Is Critical for the Recruitment of Mesenchymal Stem Cells to the Fracture Site during Skeletal Repair in a Mouse Model. *Arthritis Rheum.* **2009**, *60*, 813–823, doi:10.1002/art.24330.

64. Wan, M.; Li, C.; Zhen, G.; Jiao, K.; He, W.; Jia, X.; Wang, W.; Shi, C.; Xing, Q.; Chen, Y.-F.; et al. Injury-Activated Transforming Growth Factor β Controls Mobilization of Mesenchymal Stem Cells for Tissue Remodeling. *Stem Cells Dayt. Ohio* **2012**, *30*, 2498–2511, doi:10.1002/stem.1208.
65. Fitzsimmons, R.E.B.; Mazurek, M.S.; Soos, A.; Simmons, C.A. Mesenchymal Stromal/Stem Cells in Regenerative Medicine and Tissue Engineering. *Stem Cells Int.* **2018**, *2018*, 8031718, doi:10.1155/2018/8031718.
66. Calabrese, G.; Giuffrida, R.; Forte, S.; Fabbi, C.; Figallo, E.; Salvatorelli, L.; Memeo, L.; Parenti, R.; Gulisano, M.; Gulino, R. Human Adipose-Derived Mesenchymal Stem Cells Seeded into a Collagen-Hydroxyapatite Scaffold Promote Bone Augmentation after Implantation in the Mouse. *Sci. Rep.* **2017**, *7*, 7110, doi:10.1038/s41598-017-07672-0.
67. Iaquinta, M.R.; Torreggiani, E.; Mazziotta, C.; Ruffini, A.; Sprio, S.; Tampieri, A.; Tognon, M.; Martini, F.; Mazzoni, E. In Vitro Osteoinductivity Assay of Hydroxylapatite Scaffolds, Obtained with Biomorphic Transformation Processes, Assessed Using Human Adipose Stem Cell Cultures. *Int. J. Mol. Sci.* **2021**, *22*, 7092, doi:10.3390/ijms22137092.
68. Mohseny, A.B.; Machado, I.; Cai, Y.; Schaefer, K.-L.; Serra, M.; Hogendoorn, P.C.W.; Llombart-Bosch, A.; Cleton-Jansen, A.-M. Functional Characterization of Osteosarcoma Cell Lines Provides Representative Models to Study the Human Disease. *Lab. Invest.* **2011**, *91*, 1195–1205, doi:10.1038/labinvest.2011.72.
69. Pautke, C.; Schieker, M.; Tischer, T.; Kolk, A.; Neth, P.; Mutschler, W.; Milz, S. Characterization of Osteosarcoma Cell Lines MG-63, Saos-2 and U-2 OS in Comparison to Human Osteoblasts. *Anticancer Res.* **2004**, *24*, 3743–3748.
70. Lucero, C.M.J.; Vega, O.A.; Osorio, M.M.; Tapia, J.C.; Antonelli, M.; Stein, G.S.; Van Wijnen, A.J.; Galindo, M.A. The Cancer-Related Transcription Factor Runx2 Modulates Cell Proliferation in Human Osteosarcoma Cell Lines. *J. Cell. Physiol.* **2013**, *228*, 10.1002/jcp.24218, doi:10.1002/jcp.24218.
71. Du, L.; Fan, Q.; Tu, B.; Yan, W.; Tang, T. Establishment and Characterization of a New Highly Metastatic Human Osteosarcoma Cell Line Derived from Saos2. *Int. J. Clin. Exp. Pathol.* **2014**, *7*, 2871–2882.
72. Rodan, S.B.; Imai, Y.; Thiede, M.A.; Wesolowski, G.; Thompson, D.; Bar-Shavit, Z.; Shull, S.; Mann, K.; Rodan, G.A. Characterization of a Human

Osteosarcoma Cell Line (Saos-2) with Osteoblastic Properties. *Cancer Res.* **1987**, *47*, 4961–4966.

73. Campioni, K.; Morelli, C.; Trevisiol, L.; Nocini, P.F.; Manfrini, M.; Tognon, M. *Novel Engineered Human Fluorescent Osteoblasts for Scaffolds Bioassays*; 2010;
74. Manfrini, M.; Mazzoni, E.; Barbanti-Brodano, G.; Nocini, P.; D'agostino, A.; Trombelli, L.; Tognon, M. Osteoconductivity of Complex Biomaterials Assayed by Fluorescent-Engineered Osteoblast-like Cells. *Cell Biochem. Biophys.* **2015**, *71*, 1509–1515, doi:10.1007/s12013-014-0374-x.
75. Morelli, C.; Barbanti-Brodano, G.; Ciannilli, A.; Campioni, K.; Boriani, S.; Tognon, M. Cell Morphology, Markers, Spreading, and Proliferation on Orthopaedic Biomaterials. An Innovative Cellular Model for the "in Vitro" Study. *J. Biomed. Mater. Res. A* **2007**, *83*, 178–183, doi:10.1002/jbm.a.31262.
76. Tognon, M.; Morelli, C.; Ciannilli, A.; Campioni, K.; Di Bona, C.; Boriani, S.; Barbanti Brodano, G. A Novel Genetically Engineered Human Osteoblasts for the in Vitro Study of Biomaterials. *Top. Tissue Eng.* **2008**, 261–280.
77. Globig, P.; Willumeit-Römer, R.; Martini, F.; Mazzoni, E.; Luthringer-Feyerabend, B.J.C. Slow Degrading Mg-Based Materials Induce Tumor Cell Dormancy on an Osteosarcoma-Fibroblast Coculture Model. *Bioact. Mater.* **2021**, doi:10.1016/j.bioactmat.2021.12.031.
78. Zhu, Y.; Ouyang, Y.; Chang, Y.; Luo, C.; Xu, J.; Zhang, C.; Huang, W. Evaluation of the Proliferation and Differentiation Behaviors of Mesenchymal Stem Cells with Partially Converted Borate Glass Containing Different Amounts of Strontium in Vitro. *Mol. Med. Rep.* **2013**, *7*, 1129–1136, doi:10.3892/mmr.2013.1341.
79. Giorgi, C.; Bonora, M.; Missiroli, S.; Poletti, F.; Ramirez, F.G.; Morciano, G.; Morganti, C.; Pandolfi, P.P.; Mammano, F.; Pinton, P. Intravital Imaging Reveals P53-Dependent Cancer Cell Death Induced by Phototherapy via Calcium Signaling. *Oncotarget* **2014**, *6*, 1435–1445.
80. Bi, D.; Li, X.; Li, T.; Li, X.; Lin, Z.; Yao, L.; Li, H.; Xu, H.; Hu, Z.; Zhang, Z.; et al. Characterization and Neuroprotection Potential of Seleno-Polymannuronate. *Front. Pharmacol.* **2020**, *11*, 21, doi:10.3389/fphar.2020.00021.
81. Kim, M.; Kim, D.-I.; Kim, E.K.; Kim, C.-W. CXCR4 Overexpression in Human Adipose Tissue-Derived Stem Cells Improves Homing and Engraftment in an

Animal Limb Ischemia Model. *Cell Transplant.* **2017**, *26*, 191–204, doi:10.3727/096368916X692708.

82. Lisi, A.; Briganti, E.; Ledda, M.; Losi, P.; Grimaldi, S.; Marchese, R.; Soldani, G. A Combined Synthetic-Fibrin Scaffold Supports Growth and Cardiomyogenic Commitment of Human Placental Derived Stem Cells. *PloS One* **2012**, *7*, e34284, doi:10.1371/journal.pone.0034284.
83. Eilenberger, C.; Kratz, S.R.A.; Rothbauer, M.; Ehmoser, E.-K.; Ertl, P.; Küpcü, S. Optimized AlamarBlue Assay Protocol for Drug Dose-Response Determination of 3D Tumor Spheroids. *MethodsX* **2018**, *5*, 781–787, doi:10.1016/j.mex.2018.07.011.
84. Kazantseva, L.; Becerra, J.; Santos-Ruiz, L. Oridonin Enhances Antitumor Effects of Doxorubicin in Human Osteosarcoma Cells. *Pharmacol. Rep.* **2021**, doi:10.1007/s43440-021-00324-1.
85. Sharma, N.; Arya, G.; Kumari, R.M.; Gupta, N.; Nimesh, S. Evaluation of Anticancer Activity of Silver Nanoparticles on the A549 Human Lung Carcinoma Cell Lines through Alamar Blue Assay. *Bio-Protoc.* **2019**, *9*, e3131, doi:10.21769/BioProtoc.3131.
86. Ren, J.; Jin, P.; Sabatino, M.; Balakumaran, A.; Feng, J.; Kuznetsov, S.A.; Klein, H.G.; Robey, P.G.; Stroncek, D.F. Global Transcriptome Analysis of Human Bone Marrow Stromal Cells (BMSC) Reveals Proliferative, Mobile and Interactive Cells That Produce Abundant Extracellular Matrix Proteins, Some of Which May Affect BMSC Potency. *Cytotherapy* **2011**, *13*, 661–674, doi:10.3109/14653249.2010.548379.
87. Paiva, K.B.S.; Granjeiro, J.M. Matrix Metalloproteinases in Bone Resorption, Remodeling, and Repair. *Prog. Mol. Biol. Transl. Sci.* **2017**, *148*, 203–303, doi:10.1016/bs.pmbts.2017.05.001.
88. Wedepohl, S.; Dernedde, J.; Vahedi-Faridi, A.; Tauber, R.; Saenger, W.; Bulut, H. Reducing Macro- and Microheterogeneity of N-Glycans Enables the Crystal Structure of the Lectin and EGF-Like Domains of Human L-Selectin To Be Solved at 1.9 Å Resolution. *Chembiochem Eur. J. Chem. Biol.* **2017**, *18*, 1338–1345, doi:10.1002/cbic.201700220.
89. Midgley, A.C.; Rogers, M.; Hallett, M.B.; Clayton, A.; Bowen, T.; Phillips, A.O.; Steadman, R. Transforming Growth Factor-B1 (TGF-B1)-Stimulated Fibroblast to Myofibroblast Differentiation Is Mediated by Hyaluronan (HA)-Facilitated

Epidermal Growth Factor Receptor (EGFR) and CD44 Co-Localization in Lipid Rafts. *J. Biol. Chem.* **2013**, *288*, 14824–14838, doi:10.1074/jbc.M113.451336.

90. Di Benedetto, A.; Brunetti, G.; Posa, F.; Ballini, A.; Grassi, F.R.; Colaianni, G.; Colucci, S.; Rossi, E.; Cavalcanti-Adam, E.A.; Lo Muzio, L.; et al. Osteogenic Differentiation of Mesenchymal Stem Cells from Dental Bud: Role of Integrins and Cadherins. *Stem Cell Res.* **2015**, *15*, 618–628, doi:10.1016/j.scr.2015.09.011.
91. Docheva, D.; Popov, C.; Alberton, P.; Aszodi, A. Integrin Signaling in Skeletal Development and Function. *Birth Defects Res. Part C Embryo Today Rev.* **2014**, *102*, 13–36, doi:10.1002/bdrc.21059.
92. Saito, M.; Marumo, K. Effects of Collagen Crosslinking on Bone Material Properties in Health and Disease. *Calcif. Tissue Int.* **2015**, *97*, 242–261, doi:10.1007/s00223-015-9985-5.
93. Wu, J.; Ren, W.; Zheng, Z.; Huang, Z.; Liang, T.; Li, F.; Shi, Z.; Jiang, Q.; Yang, X.; Guo, L. Mmu_circ_003795 Regulates Osteoblast Differentiation and Mineralization in MC3T3-E1 and MDPC23 by Targeting COL15A1. *Mol. Med. Rep.* **2020**, *22*, 1737–1746, doi:10.3892/mmr.2020.11264.
94. Skandalis, S.S.; Karalis, T.; Heldin, P. Intracellular Hyaluronan: Importance for Cellular Functions. *Semin. Cancer Biol.* **2020**, *62*, 20–30, doi:10.1016/j.semcancer.2019.07.002.
95. Mead, T.J.; Apte, S.S. ADAMTS Proteins in Human Disorders. *Matrix Biol. J. Int. Soc. Matrix Biol.* **2018**, *71–72*, 225–239, doi:10.1016/j.matbio.2018.06.002.
96. Przemyslaw, L.; Boguslaw, H.A.; Elzbieta, S.; Malgorzata, S.M. ADAM and ADAMTS Family Proteins and Their Role in the Colorectal Cancer Etiopathogenesis. *BMB Rep.* **2013**, *46*, 139–150, doi:10.5483/BMBRep.2013.46.3.176.
97. Milner, J.M.; Cawston, T.E. Matrix Metalloproteinase Knockout Studies and the Potential Use of Matrix Metalloproteinase Inhibitors in the Rheumatic Diseases. *Curr. Drug Targets Inflamm. Allergy* **2005**, *4*, 363–375, doi:10.2174/1568010054022141.
98. Liang, H.P.H.; Xu, J.; Xue, M.; Jackson, C.J. Matrix Metalloproteinases in Bone Development and Pathology: Current Knowledge and Potential Clinical Utility. *Met. Med.* **2016**, *3*, 93–102, doi:10.2147/MNM.S92187.
99. Sasano, Y.; Zhu, J.-X.; Tsubota, M.; Takahashi, I.; Onodera, K.; Mizoguchi, I.; Kagayama, M. Gene Expression of MMP8 and MMP13 during Embryonic

Development of Bone and Cartilage in the Rat Mandible and Hind Limb. *J. Histochem. Cytochem. Off. J. Histochem. Soc.* **2002**, *50*, 325–332, doi:10.1177/002215540205000304.

100. Bord, S.; Horner, A.; Hembry, R.M.; Compston, J.E. Stromelysin-1 (MMP-3) and Stromelysin-2 (MMP-10) Expression in Developing Human Bone: Potential Roles in Skeletal Development. *Bone* **1998**, *23*, 7–12, doi:10.1016/S8756-3282(98)00064-7.
101. Ortega, N.; Behonick, D.J.; Werb, Z. Matrix Remodeling during Endochondral Ossification. *Trends Cell Biol.* **2004**, *14*, 86–93, doi:10.1016/j.tcb.2003.12.003.
102. Reyes, R.; Rodríguez, J.A.; Orbe, J.; Arnau, M.R.; Évora, C.; Delgado, A. Combined Sustained Release of BMP2 and MMP10 Accelerates Bone Formation and Mineralization of Calvaria Critical Size Defect in Mice. *Drug Deliv.* **2018**, *25*, 750–756, doi:10.1080/10717544.2018.1446473.
103. Lanzillotti, C.; De Mattei, M.; Mazziotta, C.; Taraballi, F.; Rotondo, J.C.; Tognon, M.; Martini, F. Long Non-Coding RNAs and MicroRNAs Interplay in Osteogenic Differentiation of Mesenchymal Stem Cells. *Front. Cell Dev. Biol.* **2021**, *9*, doi:10.3389/fcell.2021.646032.
104. Martini, F.; Pellati, A.; Mazzoni, E.; Salati, S.; Caruso, G.; Contartese, D.; De Mattei, M. Bone Morphogenetic Protein-2 Signaling in the Osteogenic Differentiation of Human Bone Marrow Mesenchymal Stem Cells Induced by Pulsed Electromagnetic Fields. *Int. J. Mol. Sci.* **2020**, *21*, E2104, doi:10.3390/ijms21062104.
105. Iaquinta, M.R.; Lanzillotti, C.; Mazziotta, C.; Bononi, I.; Frontini, F.; Mazzoni, E.; Oton-Gonzalez, L.; Rotondo, J.C.; Torreggiani, E.; Tognon, M.; et al. The Role of MicroRNAs in the Osteogenic and Chondrogenic Differentiation of Mesenchymal Stem Cells and Bone Pathologies. *Theranostics* **2021**.
106. Hojo, H.; Ohba, S.; Yano, F.; Saito, T.; Ikeda, T.; Nakajima, K.; Komiyama, Y.; Nakagata, N.; Suzuki, K.; Takato, T.; et al. Gli1 Protein Participates in Hedgehog-Mediated Specification of Osteoblast Lineage during Endochondral Ossification. *J. Biol. Chem.* **2012**, *287*, 17860–17869, doi:10.1074/jbc.M112.347716.
107. Larsen, K.H.; Frederiksen, C.M.; Burns, J.S.; Abdallah, B.M.; Kassem, M. Identifying a Molecular Phenotype for Bone Marrow Stromal Cells with in Vivo

Bone-Forming Capacity. *J. Bone Miner. Res. Off. J. Am. Soc. Bone Miner. Res.* **2010**, *25*, 796–808, doi:10.1359/jbmr.091018.

108. Meng, B.; Wu, D.; Cheng, Y.; Huang, P.; Liu, Y.; Gan, L.; Liu, C.; Cao, Y. Interleukin-20 Differentially Regulates Bone Mesenchymal Stem Cell Activities in RANKL-Induced Osteoclastogenesis through the OPG/RANKL/RANK Axis and the NF-KB, MAPK and AKT Signalling Pathways. *Scand. J. Immunol.* **2020**, *91*, e12874, doi:10.1111/sji.12874.
109. Li, Y.; Deng, Z.; Zeng, C.; Lei, G. Role of Osteopontin in Osteosarcoma. *Med. Oncol.* **2014**, *32*, 449, doi:10.1007/s12032-014-0449-y.
110. Luo, X.; Chen, J.; Song, W.-X.; Tang, N.; Luo, J.; Deng, Z.-L.; Sharff, K.A.; He, G.; Bi, Y.; He, B.-C.; et al. Osteogenic BMPs Promote Tumor Growth of Human Osteosarcomas That Harbor Differentiation Defects. *Lab. Investig. J. Tech. Methods Pathol.* **2008**, *88*, 1264–1277, doi:10.1038/labinvest.2008.98.
111. Kansara, M.; Teng, M.W.; Smyth, M.J.; Thomas, D.M. Translational Biology of Osteosarcoma. *Nat. Rev. Cancer* **2014**, *14*, 722–735, doi:10.1038/nrc3838.
112. Suksiriworapong, J.; Taresco, V.; Ivanov, D.P.; Styliari, I.D.; Sakchaisri, K.; Junyaprasert, V.B.; Garnett, M.C. Synthesis and Properties of a Biodegradable Polymer-Drug Conjugate: Methotrexate-Poly(Glycerol Adipate). *Colloids Surf. B Biointerfaces* **2018**, *167*, 115–125, doi:10.1016/j.colsurfb.2018.03.048.
113. Zhou, Z.-F.; Sun, T.-W.; Chen, F.; Zuo, D.-Q.; Wang, H.-S.; Hua, Y.-Q.; Cai, Z.-D.; Tan, J. Calcium Phosphate-Phosphorylated Adenosine Hybrid Microspheres for Anti-Osteosarcoma Drug Delivery and Osteogenic Differentiation. *Biomaterials* **2017**, *121*, 1–14, doi:10.1016/j.biomaterials.2016.12.031.
114. Sramek, M.; Neradil, J.; Sterba, J.; Veselska, R. Non-DHFR-Mediated Effects of Methotrexate in Osteosarcoma Cell Lines: Epigenetic Alterations and Enhanced Cell Differentiation. *Cancer Cell Int.* **2016**, *16*, 14, doi:10.1186/s12935-016-0289-2.
115. Choi, E.W.; Shin, I.S.; Song, J.W.; Lee, M.; Yun, T.W.; Yang, J.; Choi, K.-S.; Kim, S.-J. Effects of Transplantation of CTLA4Ig-Overexpressing Adipose Tissue-Derived Mesenchymal Stem Cells in Mice With Sustained Severe Rheumatoid Arthritis. *Cell Transplant.* **2016**, *25*, 243–259, doi:10.3727/096368915X688470.

116. Stepanenko, A.A.; Dmitrenko, V.V. Pitfalls of the MTT Assay: Direct and off-Target Effects of Inhibitors Can Result in over/Underestimation of Cell Viability. *Gene* **2015**, *574*, 193–203, doi:10.1016/j.gene.2015.08.009.

SCIENTIFIC CONTRIBUTIONS

During my PhD studies I gave my contribution working in different researches, shared with different investigators, which were based on common scientific interests. Specifically, my investigations concerned the Regenerative Medicine and Molecular Oncology fields, which were **published** in distinct Scientific Journals, as reported below:

1. Rotondo JC, Mazziotta C, **Lanzillotti C**, Tognon M, Martini F. **Epigenetic dysregulations in Merkel cell polyomavirus-driven Merkel cell carcinoma**. International journal of Molecular Sciences, 2021. doi: 10.3390/ijms222111464. Impact Factor (IF) JCR 2020= 5.923.

2. Mazziotta C, **Lanzillotti C**, Govoni M, Pellielo G, Mazzoni E, Tognon M, Martini F, Rotondo JC. **Decreased prevalence of IgG antibodies reacting to viral protein mimotopes of oncogenic Merkel cell polyomavirus in sera from healthy elderly subjects**. Frontiers in Immunology, Viral Immunology. 2021. doi: 10.3389/fimmu.2021.738486. Impact Factor (IF) JCR 2020=6.429

3. Mazziotta C, Rotondo JC, **Lanzillotti C**, Campione G, Martini F and Tognon M. **Cancer biology and molecular genetics of A3 adenosine receptor.** Oncogene. 2021. doi: 10.1038/s41388-021-02090-z. Impact Factor (IF) JCR 2020= 9.867

4. Rotondo JC, Martini F, Maritati M, Mazziotta C, Di Mauro G, **Lanzillotti C**, Barp N, Gallerani A, Tognon M, Contini C. **SARS-CoV-2 infection: new molecular, phylogenetic, and pathogenetic insights. Safety of current vaccines and the potential risk of variants**. Viruses 2021, 13(9). doi.org/10.3390/v13091687. Impact Factor (IF) JCR 2020=5.048

5. Oton-Gonzalez L, Rotondo JC, **Lanzillotti C**, Mazzoni E, Bononi I, Iaquinta MR, Cerritelli L, Malagutti N, Ciorba A, Bianchini C, Pelucchi S, Tognon M, Martini F., **Serum HPV16 E7 oncoprotein is a recurrence marker of Oropharyngeal Squamous Cell carcinomas.** Cancers Biomarkers. 2021. doi.org/10.3390/cancers13133370 6.639. Impact Factor (IF) JCR 2020= 6.639.

6. Rotondo JC, **Lanzillotti C**, Mazziotta C, Tognon M, Martini F. **Epigenetics of male infertility: the role of DNA methylation**. Frontiers in Cell and Developmental biology. 2021. doi: 10.3389/fcell.2021.689624. Impact Factor (IF) JCR 2020= 6.684.

7. Mazziotta C, **Lanzillotti C**, Torreggiani E, Oton-Gonzalez L, Iaquinta MR, Mazzoni E, Gaboriaud P, Touzé A, Silvagni E, Govoni M, Martini F, Tognon M, Rotondo JC. **Serum antibodies against the oncogenic Merkel Cell Polyomavirus detected by an innovative immunological assay with mimotopes in healthy subjects**. Frontiers in Immunology. 2021. doi.org/10.3389/fimmu.2021.676627. Impact Factor (IF) JCR 2020= 7.561.

8. Iaquinta MR*, **Lanzillotti C***, Mazziotta C*, Bononi I, Frontini F, Mazzoni E, Oton-Gonzalez L, Rotondo JC, Torreggiani E, Tognon M, Martini F. **The role of microRNAs in the osteogenic and chondrogenic differentiation of mesenchymal stem cells and bone pathologies**. Theranostics, Vol. 11, No. 13, **2021**. doi:10.7150/thno.55664. Impact Factor (IF) JCR 2020= 11.556.

9. **Lanzillotti C**, De Mattei M, Mazziotta C, Taraballi F, Rotondo JC, Tognon M, Martini F. **Long non-coding RNAs and microRNAs interplay in osteogenic differentiation of mesenchymal stem cells**. Frontiers in Cell and Developmental biology, **2021**. doi: 10.3389/fcell.2021.646032. Impact Factor (IF) JCR 2020= 6.684.

10. Mazziotta C*, **Lanzillotti C***, Iaquinta MR*, Taraballi F, Torreggiani E, Rotondo JC, Oton-Gonzalez L, Mazzoni E, Frontini F, Bononi I, De Mattei M, Tognon M, Martini F. **MicroRNAs regulate signaling pathways in osteogenic differentiation of mesenchymal stem cells**. International journal

of Molecular Sciences, Vol. 22, No. 5, **2021**. doi: 10.3390/ijms22052362. Impact Factor (IF) JCR 2020= 5.923.

11. Mazzoni E, Iaquinta MR, **Lanzillotti C**, Mazziotta C, Maritati M, Montesi M, Sprio S, Tampieri A, Tognon M, Martini F. **Bioactive materials for soft tissue repair**. Frontiers Bioengineering and Biotechnology, Vol. 9, No. 1, pp: 1-17, **2021**. doi: 10.3389/fbioe.2021.613787. Impact Factor (IF) JCR 2020= 5.890.

12. Oton-Gonzalez L, Rotondo JC, Cerritelli L, Malagutti N**, Lanzillotti C**, Bononi I, Ciorba A, Bianchini C, Mazziotta C, De Mattei M, Pelucchi S, Tognon M, Martini F. **Association between HPV infection and Killian polyp**, Infectious Agents and Cancer, Vol. 16, No. 1, pp: 1-9, **2021**. doi.org/10.1186/s13027-020-00342-3. Impact Factor (IF) JCR 2019= 2.74.

13. Mazzoni E, Mazziotta C, Iaquinta MR, **Lanzillotti C**, D'Agostino A, Trevisiol L, Tognon M, Martini F. **Enhanced Osteogenic Differentiation of Human Bone Marrow-Derived Mesenchymal Stem Cells by a Hybrid Hydroxylapatite/Collagen Scaffold**. Frontiers Cell and Developmental Biology, Vol. 8, No. 1, pp: 610570-610570, **2021**. doi:10.3389/fcell.2020.610570. Impact Factor (IF) JCR 2020= 6.684.

14. Rotondo JC, Oton-Gonzalez L, Mazziotta C, **Lanzillotti C**, Iaquinta MR, Tognon M, Martini F. **Simultaneous detection and viral DNA load quantification of different Human Papillomavirus types in clinical specimens by the high analytical droplet digital PCR method**. Frontiers in Microbiology, Vol. 11, pp: 1-14, **2020**. doi: 10.3389/fmicb.2020.591452. Impact Factor (IF) JCR 2020= 5.640.

15. Corazza M, Oton-Gonzalez L, Scudieri V, Rotondo JC, **Lanzillotti C**, Di Mauro G, Tognon M, Martini F, Borghi A. **Tissue cytokine/chemokine profile in vulvar lichen sclerosus: an observational study on keratinocyte and fibroblast cultures**. Journal of Dermatological Science, Vol. S0923-

1811, No. 20, pp: 30295-30299, **2020**. doi: 10.1016/j.jdermsci.2020.09.006. Impact Factor (IF) JCR 2020= 4.563.

16. Rotondo JC, Oton-Gonzalez L, Selvatici R, Rizzo P, Pavasini R, Campo GC, **Lanzillotti C**, Mazziotta C, De Mattei M, Tognon M, Martini F. **SERPINA1 gene promoter is differentially methylated in peripheral blood mononuclear cells of pregnant women**. Frontiers in Cell and Developmental biology, Vol. 8, No. 1, **2020**. doi: 10.3389/fcell.2020.550543. Impact Factor (IF) JCR 2020= 6.684.

17. Tognon M, Tagliapietra A, Magagnoli F, Mazziotta C, Oton-Gonzalez L, **Lanzillotti C**, Contini C, Vesce F, Rotondo JC, Martini F. **Investigation on spontaneous abortion and Human Papillomavirus infection**. Vaccines, Vol. 8, No. 3, pp: 1-14, **2020**. doi: 10.3390/vaccines8030473. Impact Factor (IF) JCR 2020=4.422.

18. Mazzoni E, Pellegrinelli E, Mazziotta C, **Lanzillotti C**, Rotondo JC, Bononi I, Iaquinta MR, Manfrini M, Vesce F, Tognon M, Martini F. **Mother-to-child transmission of oncogenic polyomaviruses BKPyV, JCPyV and SV40**. Journal of Infection, Vol. 80, No. 5, pp: 563-570, **2020**. doi: 10.1016/j.jinf.2020.02.006. Impact Factor (IF) JCR 2020= 6.072.

19. Mazziotta C, **Lanzillotti C**, Gafà R, Touzé A, Durand MA, Martini F, Rotondo JC. **The role of histone post-translational modifications in Merkel cell carcinoma**. Front. Oncol. 2022. Accepted; doi: pending. Impact Factor (IF) JCR 2020= 6.244

20. Rotondo JC, Mazziotta C, Lanzillotti C, Stefani C, Campione G, Tognon M, Martini F. **The Role of Purinergic P2X7 Receptor in inflammation and cancer**. Cancers 2022. Under review. Impact Factor (IF) JCR 2020= 6.162

My experimental activities were designed on the basis of two main investigations carried out over the past three years, as a PhD student. Together with already published articles/reviews I plan to write two different additional articles that are now **in preparation**, such as:

1. **Lanzillotti C** et al., *New delivery system represented by an osteoinductive scaffold with methotrexate/doxorubicin as a novel therapeutic strategy against osteosarcoma.*
2. **Lanzillotti C** et al., *Retinoic Acid Receptor β pathway tested dysregulated in HPV-driven Cervical Intraepithelial Neoplasia keratinocytes*.

Università degli Studi di Ferrara

Sezioni

Dottorati di ricerca

Il tuo indirizzo e-mail

lnzcmn@unife.it

Oggetto:

Dichiarazione di conformità della tesi di Dottorato

Io sottoscritto Dott. (Cognome e Nome)

Lanzillotti Carmen

Nato a:

Ostuni

Provincia:

Brindisi

Il giorno:

30/01/1994

Avendo frequentato il Dottorato di Ricerca in:

Medicina Molecolare

Ciclo di Dottorato

34

Titolo della tesi:

Innovative drug delivery scaffolds as novel therapeutic strategy for bone tissue regeneration and treatment of osteosarcoma

Titolo della tesi (traduzione):

Biomateriali innovativi con sistema di rilascio di farmaci come nuova strategia terapeutica per la rigenerazione del tessuto osseo e il trattamento dell'osteosarcoma

Tutore: Prof. (Cognome e Nome)

Martini Fernanda

Settore Scientifico Disciplinare (S.S.D.)

BIO/13

Parole chiave della tesi (max 10):

Cellule staminali, SAOS, biomateriale, sistema di rilascio di farmaci, osso, osteosarcoma, osteogenesi, medicina rigenerativa, Stem cell, SAOS, scaffold, drug-delivery, bone, osteosarcoma, osteogenesis, regenerative medicine

Consapevole, dichiara

CONSAPEVOLE: (1) del fatto che in caso di dichiarazioni mendaci, oltre alle sanzioni previste dal codice penale e dalle Leggi speciali per l'ipotesi di falsità in atti ed uso di atti falsi, decade fin dall'inizio e senza necessità di alcuna formalità dai benefici conseguenti al provvedimento emanato sulla base di tali dichiarazioni; (2) dell'obbligo per l'Università di provvedere al deposito di legge delle tesi di dottorato al

fine di assicurarne la conservazione e la consultabilità da parte di terzi; (3) della procedura adottata dall'Università di Ferrara ove si richiede che la tesi sia consegnata dal dottorando in 2 copie, di cui una in formato cartaceo e una in formato pdf non modificabile su idonei supporti (CD-ROM, DVD) secondo le istruzioni pubblicate sul sito : http://www.unife.it/studenti/dottorato alla voce ESAME FINALE – disposizioni e modulistica; (4) del fatto che l'Università, sulla base dei dati forniti, archivierà e renderà consultabile in rete il testo completo della tesi di dottorato di cui alla presente dichiarazione attraverso l'Archivio istituzionale ad accesso aperto "EPRINTS.unife.it" oltre che attraverso i Cataloghi delle Biblioteche Nazionali Centrali di Roma e Firenze. DICHIARO SOTTO LA MIA RESPONSABILITA': (1) che la copia della tesi depositata presso l'Università di Ferrara in formato cartaceo è del tutto identica a quella presentata in formato elettronico (CD-ROM, DVD), a quelle da inviare ai Commissari di esame finale e alla copia che produrrà in seduta d'esame finale. Di conseguenza va esclusa qualsiasi responsabilità dell'Ateneo stesso per quanto riguarda eventuali errori, imprecisioni o omissioni nei contenuti della tesi; (2) di prendere atto che la tesi in formato cartaceo è l'unica alla quale farà riferimento l'Università per rilasciare, a mia richiesta, la dichiarazione di conformità di eventuali copie. PER ACCETTAZIONE DI QUANTO SOPRA RIPORTATO

Dichiarazione per embargo

12 mesi

Richiesta motivata embargo

1. Tesi in corso di pubblicazione

Liberatoria consultazione dati Eprints

Consapevole del fatto che attraverso l'Archivio istituzionale ad accesso aperto "EPRINTS.unife.it" saranno comunque accessibili i metadati relativi alla tesi (titolo, autore, abstract, ecc.)

Firma del dottorando

Ferrara, li 08/03/2022 Firma del Dottorando 

Firma del Tutore

Visto: Il Tutore Si approva Firma del Tutore